HHS Public Access

Author manuscript

Neurobiol Dis. Author manuscript; available in PMC 2016 March 01.

Published in final edited form as:

Neurobiol Dis. 2015 March ; 75: 1–14. doi:10.1016/j.nbd.2014.12.013.

Metabolic Responses Differentiate between Interictal, Ictal and Persistent Epileptiform Activity in Intact, Immature Hippocampus *in vitro*

Anton I. Ivanov[#,$], **Christophe Bernard**[#,$], and **Dennis A. Turner**[*]

[#]Aix Marseille Université, INS, Marseille, France

[$]Inserm, UMR_S 1106, Marseille, France

[*]Neurosurgery and Neurobiology, Duke University Medical Center, Durham, NC 27710

Abstract

Interictal spikes, ictal responses, and status epilepticus are characteristic of abnormal neuronal activity in epilepsy. Since these events may involve different energy requirements, we evaluated metabolic function (assessed by simultaneous NADH and FAD imaging and tissue O2 recordings) in the immature, intact mouse hippocampus (P5-P7, *in vitro*) during spontaneous interictal spikes and ictal-like events (ILEs), induced by increased neuronal network excitability with either low Mg2+ media or decreased inhibition with bicuculline. In low Mg2+ medium NADH fluorescence showed a small decrease both during the interictal build-up leading to an ictal event and before ILE occurrences, but a large positive response during and after ILEs (up to 10% net change). Tissue O2 recordings (pO2) showed an oxygen dip (indicating oxygen consumption) coincident with each ILE at P5 and P7, closely matching an NADH fluorescence increase, indicating a large surge in oxidative metabolism. The ILE O2 dip was significantly larger at P7 as compared to P5 suggesting a higher metabolic response at P7. After several ILEs at P7, continuous, low voltage activity (late recurrent discharges: LRDs) occurred. During LRDs, whilst the epileptiform activity was relatively small (low voltage synchronous activity) oxygen levels remained low and NADH fluorescence elevated, indicating persistent oxygen utilization and maintained high metabolic demand. In bicuculline, NADH fluorescence levels decreased prior to the onset of epileptiform activity, followed by a slow positive phase, which persisted during interictal responses. Metabolic responses can thus differentiate between interictal, ictal-like and persistent epileptiform activity resembling status epilepticus, and confirm that spreading depression did not occur. These results demonstrate clear translational value to the understanding of metabolic requirements during epileptic conditions.

Correspondence to: Dennis A. Turner MA, MD, Box 3807, Neurosurgery, DUMC, Durham, NC 27710, Phone 919-684-6706, FAX 919-681-8068, dennis.turner@duke.edu.

Conflict of Interest: The authors declare no competing interests.

Keywords

Epilepsy; Hippocampus; Metabolism; Oxygen; In Vitro Preparations

Introduction

Epileptogenic brain regions display altered metabolism associated with structural damage, cell loss, or changes in vascular supply (Pan et al. 2008, Alavi et al. 2011). The increased energy demand associated with ictal activity is usually matched with an appropriate metabolic response (Duffy et al. 1975, Chapman et al. 1977, Folbergrova et al. 1985). For example, fluorodeoxyglucose (FDG) PET scans in humans show basal hypometabolic regions between seizure events, which convert to hypermetabolic conditions during and after a seizure (Pan et al. 2008, Alavi et al. 2011). The metabolic demands associated with interictal and ictal epileptiform events can be estimated in animal models using fluorescent FAD+ or NADH metabolic recordings (O'Connor et al. 1972, Schuchmann et al. 1999, Kovacs et al. 2001, Heinemann et al. 2002, Heinemann et al. 2002, Kann et al. 2005) (Dora 1983) (Cooper et al. 2009, Zhao et al. 2011)), or cytochrome analysis with oxygen recordings (Kreisman et al. 1983). Additionally, the spread of ictal events can be estimated with intrinsic optical signal changes associated with cell swelling (Holtkamp et al. 2011)). Thus, estimates of metabolic demand, particularly NADH/FAD+ imaging and tissue oxygen levels, may help differentiate epileptiform states in an exposed brain (i.e., surgical exposure), the counterpart of FDG and oxygen uptake PET scans in a closed preparation and under clinical conditions.

Whereas both cytosolic and mitochondrial pathways generate the critical metabolic co-factor NADH (nicotinamide adenine nucleotide), metabolic $FADH_2$ pathways and O_2 consumption primarily occur within mitochondria (Foster et al. 2005, McKenna et al. 2006, Shetty et al. 2012). Fluorescence of either NADH (at 460 nm) (Aubin 1979, Kasischke et al. 2011) or FAD+ (at 515 nm) (Zhao et al. 2011) can be used to monitor energy metabolism (Foster et al. 2005, Galeffi et al. 2007, Galeffi et al. 2011). NADH fluorescence levels also indirectly reflect oxygen availability to a critical inflection point (near 7.5 mm Hg O2), below which most NAD+ is converted to NADH (Erecinska and Silver 2001, Galeffi et al. 2011, Kasischke et al. 2011). Hence, NADH imaging and direct O2 tissue levels together provide an integrated estimate of neuronal metabolism. For example, in *in vitro* brain preparations (i.e., with no circulatory perfusion or hemodynamic response but with constant oxygen diffusion into the tissue) increased oxygen demand in the tissue leads to a lowered oxygen tension (Foster et al. 2005, Galeffi et al. 2007, Galeffi et al. 2011). Conversely, if oxygen demand is reduced (i.e., from cell death), the tissue oxygen tension can rise above baseline tissue levels (Foster et al. 2005). Depending on oxygen availability, heightened oxygen demand and utilization may be associated with either an NADH fluorescence decrease (i.e., a decreased NADH/NAD+ ratio) or an increase (Turner et al. 2007, Galeffi et al. 2011, Shetty et al. 2014). Thus, tissue oxygen recordings in concert with NADH/FAD+ imaging can reveal the level of ongoing oxidative metabolism. However, the pattern of oxygen responses differs significantly between intact (Kreisman et al. 1981) and *in vitro*

preparations (Foster et al. 2005) because the delivery of oxygen is different (active transport by blood circulation vs passive diffusion from artificial cerebrospinal fluid, respectively).

Seizure-like events (SLEs) can be induced *in vitro* with a variety of procedures, including nominally zero Mg^{2+} conditions (Mody et al. 1987, Dreier and Heinemann 1991, Gloveli et al. 1995), GABA-A antagonists (Cooper et al. 2009), and *voltage gated potassium channel blockers* [*ie, 4-aminopyridine*] (Schuchmann et al. 1999, Kibler and Durand 2011). These models of epileptiform activity display interictal-like events (IEs), SLEs (Gloveli et al. 1995, Heinemann et al. 2002), and late recurrent discharges (LRDs) reminiscent of status epilepticus (Dreier and Heinemann 1991, Schuchmann et al. 1999). Such patterns are similar to those induced *in vivo* (Chapman et al. 1977, Dora 1983, Folbergrova et al. 1985). The intact, immature hippocampus (*in vitro*) also demonstrates IEs, SLEs and LRDs in zero Mg2+ conditions (Quilichini et al. 2002, Quilichini et al. 2003, Dzhala et al. 2010, Quilichini et al. 2012). Clarifying energy metabolism during these various activities may provide a framework for the design of treatments which could prevent seizure-induced damage (Chen et al. 2007). We have used the intact immature hippocampus preparation *in vitro* for these studies because it preserves the hippocampal circuitry compared to brain slices (Schwartzkroin 1986), whilst remaining easily amenable to imaging and electrophysiological recordings.

Our hypotheses center on metabolic conditions underlying these epileptiform events, particularly that metabolic differences in tissue maturity underlay the transition to late recurrent depolarizations (LRDs) in P7 (more mature) hippocampus, that LRD occurrence is a nonconvulsive status response rather than a spreading depression response, and that there are critical differences in the metabolic responses to bicuculline (with disinhibition) and low Mg2+ conditions (with enhanced excitatory drive, particularly NMDA-mediated). To assess these hypotheses we analyzed energy metabolism (assessed by NADH/FAD+ fluorescence and tissue oxygen levels) during epileptiform events induced in low Mg2+ conditions or following blockade of fast GABAergic transmission with bicuculline. We show that metabolic activity and a moderate decrease in NADH fluorescence can precede synchronous discharge, whereas a rise in NADH tissue fluorescence and significant oxygen utilization occur together during and after epileptiform events, indicating a high level of metabolic demand. Both IE and ILE activities are similar in zero Mg2+ and bicuculline conditions with only difference in the oxidative phase, indicating that neuronal synchrony leads to intense metabolic demand. However, during LRDs in zero Mg2+ conditions NADH tissue fluorescence and oxygen utilization are considerably increased, to maintain low voltage but highly synchronized electrical activity, consistent with nonconvulsive status epilepticus.

Experimental Procedures

Immature hippocampus in vitro preparation

All protocols were designed and approved according to INSERM and international guidelines for experimental animal care and use. Experiments were performed on intact hippocampi taken from FVB NG mice between postnatal (P) day 5 and 7 (P0 was day of birth) (Quilichini et al. 2002, Quilichini et al. 2012). The immature mice were decapitated

rapidly after being cooled on ice as a temporary anaesthesia. The brain was extracted from the skull and transferred to oxygenated (95% O2 / 5% CO2) ice cold (4°C) artificial cerebrospinal fluid (aCSF) containing (in mM): NaCl 126; KCl 3.5; CaCl2 2; MgCl2 1.3; NaHCO3 25; NaHPO4 1.2; glucose 10 (pH=7.3). After at least 2 hours incubation at room temperature in aCSF, hippocampi were transferred to the recording chamber. To ensure a high perfusion rate we used a closed circuit perfusion system with recycling: 250 ml of solution were used per hippocampus and per condition. The pH (7.3) and temperature (33°C) were controlled during all experiments.

Induction of epileptiform events

Bicuculline (10 μM) was added to the ACSF after a 30 min baseline period, which generated both spontaneous interictal and ictal-like epileptiform responses (Cooper et al. 2009). In contrast, low Mg2+ media (zero added Mg2+) leads to more prolonged periods of hyperexcitability (ie, 60-90 sec) (Mody et al. 1987, Dreier and Heinemann 1991, Gloveli et al. 1995). After 30 min baseline recording in Mg2+ containing aCSF solution, the media was switched to one without added Mg2+ ion. In this condition, the extracellular concentration of Mg2+ may be influenced by other constituents of the aCSF, possibly near 0.08 mM (Mody et al. 1987). Therefore, we use the term low-Mg2+ aCSF rather than zero-Mg2+ aCSF. Because Mg2+ is a biologically active molecule for both membrane stability and enzyme activation (Altura and Altura 1996), the bicuculline condition provides an alternative mechanism for studying epileptiform activity and neuronal synchronization.

Physiological monitoring

Extracellular glass electrodes were placed into the mid CA1 region in each hippocampus, filled with low Mg2+ aCSF. The intact immature hippocampi were positioned within the chamber so that the CA1 area was up and the DG region down; the CA1 area was superficial and accessible for the recording electrodes and imaging using either transmission or epifluorescence. Local field potentials (LFPs; either spontaneous or evoked) were amplified with DAM-80 differential amplifiers (WPI) for AC-coupled recordings and a MultiClamp700B amplifier for DC-coupled recording, then digitized with a Digidata 1200B (Axon Instruments, Molecular Devices), stored on the hard drive of the personal computer and analyzed using PClamp 8.2 software (Molecular Devices). The extracellular spontaneous field potential was observed for epileptiform events.

NADH/FAD+ fluorescence imaging

NADH autofluorescence for large-scale imaging was measured using UV light emitted by a 300W pre-centered mercury lamp (Nikon Intensilight C-HGFI) passed through a fiber-optic cable and a 290-370 nm excitation filter. After trying several configurations of transmitted and refracted light angles a direct transmitted approach through the bottom of the tissue gave the best signal to noise ratio, with recordings from above the tissue using either a dissecting microscope or a lens mounted directly on the camera with the emission filter (long pass > 420 nm), due to the large field size needed to monitor the whole hippocampi (∼ 12 mm). This transmitted approach effectively averaged the NADH signal across the entire tissue depth of the intact hippocampus (∼ 1 mm). The emitted light was captured using a linear, cooled 12 bit CCD camera (PCO VGA Sensicam, Germany) equipped with 420 nm long

pass filter (Omega Optical, Brattleboro, VT, USA). Images were acquired using standard Sensicam software or ImageJ (NIH, USA).

An upright microscope with 4× lens was used for oxygen recordings, focused on the CA1 region, with NADH imaged using epifluorescence. FAD+ was imaged also in this configuration, using an excitation filter of 400-450 nm and a long-pass emission filter greater than 515 nm. The two approaches (ie, transmission fluorescence or epifluorescence) led to similar imaging responses, indicating that the CA1 area was the origin of the tissue responses.

To acquire short sequences (10-15 minutes) of rapid changes in NADH fluorescence we used 200 ms exposure time, 4Hz imaging interval, high illumination level, and 2×2 binning (with 2 ND neutral density filter). To acquire longer lasting (90-150 minutes) sequences of NADH fluorescence images we used 1600 ms exposure time, 0.5 Hz time lapse interval, no binning and low illumination (to avoid phototoxicity, 8 ND neutral density filter). Special attention was attributed to the evaluation and subtraction of the NADH signal base line, which could drift over time. For this purpose we used a 30 min recording of the base line activity in regular aCSF, which was later fit with an exponential decay function if the drift was greater than 10% in the 30 min period. This function was extrapolated to include the entire recording time and was then subtracted from each frame of the recording. Such fit and subtraction procedures were made for each hippocampus depending on the degree of NADH signal drift. The field of the camera was measured by imaging a micrometer, and each pixel varied from 11-24 μm, depending on the binning (the magnification was fixed): at 640×480 (bin = 1) the pixel size was 11μm/pixel or 94pixels/mm, whereas for 320×240 (bin of 2) there were 24 μm/pixel or 41 pixels/mm.

In these immature hippocampi transmitted UV excitation light provided an excellent fluorescent signal, since the tissue is highly translucent. To determine quantitatively the relative penetration of the UV excitation light through the tissue (< 1 mm depth total) we tested the signal arising from a highly fluorescent, opaque fragment of filter paper in the chamber, placed either above an immature hippocampus (to measure the loss due to the UV light transmission through the tissue) or just above the cover slip without the tissue in place (as a control), both conditions with aCSF media present. This quantitative comparison indicated how much UV light penetrated the full thickness of the hippocampus to excite fluorescence within the opaque filter paper, which is a worst case scenario compared to the hippocampus, where much of the UV light will excite NADH in the interior of the hippocampus. The intensity of UV light reaching the fluorescent paper over the intact hippocampus (compared to the media alone) averaged 40% compared to no hippocampus present, indicating that there is relatively good penetration across the entire hippocampus.

Regions of interest were applied to the imaging and the 12-bit values were averaged within these regions, then plotted as a function of time and directly compared to the physiological recording, using differences from the baseline just prior to the event. The 12-bit NADH images were analyzed using ImageJ (NIH, USA) by the difference from a control ROI or image, to eliminate the variable baseline fluorescence and to emphasize dynamic changes. Example images show only changes from the control to highlight the responses.

Oxygen recordings

Glass oxygen microelectrodes (10 μm, Unisense, Denmark) were calibrated and then placed superficially into the CA1 region of the middle of the immature hippocampus (ie, < 100 μm depth). Depth profiles (Foster et al. 2005, Hajos et al. 2009) were also performed to assess the basal level of oxygenation within the entire hippocampus, particularly the superficial CA1 region. Note that in this *in vitro* preparation the tissue oxygen levels are limited by diffusion, and enhanced local tissue metabolic activity leads to tissue (ie, extracellular) oxygen reduction, due to unchanged diffusion into the tissue combined with increased oxidative phosphorylation and uptake into cells (Foster et al. 2005). In contrast, if there is reduced tissue oxygen demand (i.e., due to neuronal damage or mitochondrial toxins such as oligomycin) then tissue oxygen levels increase (Erecinska and Silver 2001, Foster et al. 2006).

Statistical analysis

During incubation in low Mg2+ ACSF (70 minutes), 3 to 12 ILEs could occur. Only the first three ILEs were used to evaluate ILE-related parameters. The normality of data groups was tested with Shapiro-Francia test. If the normality was confirmed then the statistical significance was checked with one or two sample t-tests, otherwise non-parametric tests were applied (Wilcoxon signed rank one sample test, Wilcoxon Mann Whitney for two samples). Results are expressed as mean values ± SEM for the normally distributed data and median ± SEM otherwise; n is number of events observed in N experiments. In the cases where neither mean value nor median were representative (ie, a nonhomogeneous distribution) data were showed as the range between the minimal to maximal (min-max) values.

Results

Metabolic activity associated with low Mg2+ conditions at P5

Figure 1 illustrates a typical physiological response of an intact hippocampus at P5 in low Mg2+ conditions (Quilichini et al. 2002, Quilichini et al. 2003, Derchansky et al. 2004, Derchansky et al. 2006, Dzhala et al. 2008, Dzhala et al. 2010, Quilichini et al. 2012). Fig. 1A shows an example of a simultaneous recording of local field potentials (LFPs) (dark grey traces) and NADH fluorescence (black trace, from regions of interest as shown in Fig. 2). In 11 out of 14 experiments, NADH fluorescence started to decline immediately after the change in aCSF, reaching -3.8 ± 0.6 % (N = 11, Fig. 1A, B; $p < 0.001$), suggesting enhanced oxidative metabolism with the onset of hyperexcitability. After the introduction of low Mg2+, IE started to appear (in 12 out of 14 experiments), before the first ILE (Fig. 1A c1 mark; 1B detail).

In all preparations, there was a transition from IE activity to ILEs, which started with epileptiform spikes occurring at a high frequency, followed by individual bursts during the initial tonic-clonic and later clonic phase (Fig. 1, A, C1, C2). Both the initial ILE and subsequent events were accompanied by a rapid NADH fluorescence increase (5.6 ± 0.25 %; $n = 42$, $p < 0.001$) (Fig. 1A, B), which was preceded by a short (4.2 ± 0.4 s, $n=35$, $p < 0.001$) and sharp negative drop in NADH fluorescence (-0.77 ± 0.07 %, $n=35$, $p < 0.05$). In some

ILEs (7 of 42) this initial drop was not detectable due to the high level of pre-ictal activity and related ongoing NADH oxidation (example shown in Fig. 1, C1).

The onset of ILEs coincided with a large NADH fluorescence increase (time delay of 0.6 ± 0.9 s, n=42, p=0.5) defined as 2% per 10 s rise of the fluorescence (Fig. 1C1, C2). The NADH rise duration averaged 55 ± 3 s, reaching its maximal value after the end of the last population spike of the ILE then declining immediately (Fig. 1C1, C2). NADH rise duration was not different from ILE mean duration (64 ± 3 s, p = 0.22; n=42), suggesting that a high rate of NADH increase persisted during ILEs. Thus, the initial metabolic oxidation (i.e., an NADH decrease) occurred during interictal spikes preceding ILE onset, whereas the NADH overshoot began only after ILE onset and persisted throughout ILE time course. Measurements made in DC mode with an additional electrode (in 5 out of 14 experiments) revealed a small negative shift (-0.26 ± 0.8 mV, p<0.01, n=15) of the LFP baseline during each ILE (Fig. 1C1, C2, on the bottom), as previously reported (Heinemann et al. 2002, Jirsa et al. 2014). The field potential returned to baseline level within 1-3 min after ILE offset. The progressive increase in background NADH levels after recurring ILEs (Fig. 1A, noted by c2 mark) suggests a slow increase in metabolic debt arising from a lack of complete recovery after each subsequent ILE, whereas individual ILEs show similar NADH imaging characteristics (i.e., amplitude and duration) over time. *However, this is in contrast to the progressive loss or rundown of NADH responses occurring during multiple ILEs noted in hippocampal slice cultures exposed to similar low Mg2+ conditions* [Fig. 3 - (Kovacs et al. 2002)].

Figure 2 shows the detailed NADH fluorescent images from two ILEs during the experiment shown in Fig. 1; the left panel corresponds to the first ILE (Fig. 1Ac1, C1) and the right corresponds to the fifth ILE (Fig. 1Ac2, C2). The bottom graphs show the NADH response over time but with the time points of the specific images shown by tics. The control image is shown on the upper right, illustrating the single hippocampus in the chamber in a reference view; the other images are subtraction difference images, with medium gray as no change (the entire scale is ± 10%, with white representing +10% and black -10% difference). During the first ILE, NADH is slightly decreased at 34 sec (in the tip of the hippocampus) and then largely increased (white) starting at image 44 inside the darker oxidation. The other ILE (right panel) shows a more uniform pattern with only a fringe of net decrease but a prominent overshoot. The ILE responses on NADH imaging were stereotyped and very similar at both P5 and P7 to those shown. The imaging rate and slow NADH changes were insufficient to give further detail on the spread of the signal along the septo-temporal axis of each hippocampus. *Additionally, the CA1 region is in the middle of the intact hippocampus, where the signal is brightest, and the CA3 region is on the tissue edge medially* (*to the right in* Fig. 2), *indicating that most of the NADH signal arises from the CA1 region*.

Metabolic activity associated with status epilepticus-like activity at P7

Experiments performed on intact hippocampi from P7 mice showed that low Mg2+ aCSF triggered 2-5 large amplitude ILEs (Fig. 3A b1 mark, B1), followed by smaller amplitude ILEs (37 ± 2 % of the initial ILE mean amplitude; N=7; Fig. 3A b2 mark, B2). Eventually, the ILEs disappeared and small amplitude (50-400 μV) oscillations dominated, with a

frequency of 0.6-1.2 Hz (N=7, Fig. 3A, c1 mark, C1), similar to the late recurrent discharges (LRDs) recorded in both organotypic hippocampal slices and combined entorhinal-hippocampal acute slices (Dreier and Heinemann 1991, Kovacs et al. 2002, Holtkamp et al. 2011). This low voltage, persistent oscillation (Quilichini et al. 2002) persisted even after reverting to regular Mg2+ containing aCSF (Fig. 3A, c2 mark, C2). The recording in DC mode showed that, as for P5 hippocampi, each ILE was accompanied by a small, persistent negative shift (lower traces in Fig. 3 A, B1, B2) as previously reported (Heinemann et al. 2002). The electrical base line behaviour was similar to that observed at P5 when the first ILEs occurred (-1.2 ± 0.2 mV transient negative shift; N = 18, $p<0.001$). But, in P7 hippocampi, the extracellular shift became larger in amplitude (-2.2 ± 0.4 mV; N = 7, $p<0.001$) and persistent even during the last large amplitude ILE (Fig. 3A, b1 mark lower trace). As the DC shift persisted, ILE amplitude decreased (Fig. 3A b2 mark, B2,) and then LRDs emerged (Fig. 3C1, after Fig. 3A b2 mark). The DC shift did not fully recover (-2.2 ± 0.4 mV more negative than at the beginning of the experiment; N=7, $p<0.001$) even after reverting to regular aCSF (Fig. 3A, C2). Thus, LRD occurrence led to an irreversible field potential baseline shift during the persistent epileptiform activity, even after removing the epileptogenic condition. *This small DC shift occurs with ongoing electrical activity, is commonly noted with epileptiform events, likely due to synchrony amongst cell populations, and is much smaller than the DC shift heralding spreading depression* (Hablitz and Heinemann 1989, Galeffi et al. 2011).

At this stage of development (P7), the transition to Mg2+ free solution led to an increased NADH background fluorescence level during the initial interictal spiking activity prior to ILE occurrence (Fig. 3A, b1 mark). Similar to what occurred at P5, each field potential change associated with an ILE occurrence coincided with a rapid increase in NADH signal (Fig. 3A, B1, B2), which peaked until the last population spike, before decreasing. The mean amplitude of the NADH fluorescence transient corresponding to the initial ILEs was 6.29 ± 0.46 % ($p<0.001$, n=18). During subsequent ILEs, NADH increases were less pronounced (Fig. 3B2) as the DC shift was maintained, suggesting a saturation of the NADH response associated with the baseline change in extracellular field potential. Further ILEs also led to a gradual increase in baseline fluorescence, reaching a maximal value of 7.1 ± 2.5 % (N=7, $p < 0.001$) at the time of transition to LRD activity, but not in synchrony with the extracellular field, which showed a decrease at the time of LRD initiation. *As in the case of P5 hippocampus, these NADH responses are very different than those observed in hippocampal slice cultures* (Kovacs et al. 2002), *which show a progressive decline of NADH transient responses with multiple ILE occurrence, particularly after 15 ILEs*.

Thereafter, NADH fluorescence slowly decreased during LRD persistence (between Fig. 3A b2 and c1 marks), remained above baseline (3.7 ± 0.5 %; $p<0.001$, N=7), before declining to the initial level after reverting to regular aCSF (Fig. 3A c2 mark). After switching back to normal aCSF, LRDs increased in amplitude in 4/7 experiments (Fig. 3 C2 compared to C1, note the different scale). The NADH fluorescence responses suggest that at P7 the metabolic activity increased not only with each ILE occurrence but also was further enhanced during LRD initiation. However, the decrease in the NADH fluorescence during the LRD phase

suggested slow normalization of the metabolism over time in spite of persistent demand from the continuing abnormal, epileptiform activity.

Tissue oxygen recordings show persistent oxygen utilization during ILEs and LRDs

Although NADH fluorescence levels suggest enhanced oxygen utilization, in some situations increased NADH fluorescence follows a period of oxidative metabolism (as a recovery phase), and NADH fluorescence alone cannot indicate ongoing oxygen utilization (Galeffi et al. 2011). Therefore, we recorded tissue oxygen levels in the CA1 region at a depth of ~ 100 μm (Fig. 4 blue traces) together with the field responses in DC mode (Fig. 4, black traces) to determine the underlying degree of tissue oxygen utilization (Foster et al. 2005, Galeffi et al. 2011), comparing responses at P5 (upper panel) and P7 (lower panel). Oxygen levels directly parallel the NADH fluorescence responses shown above. Epileptiform activity was associated with a pronounced decrease in the tissue pO2, indicating a marked increase in oxygen utilization associated with synchronous neuronal firing but with restricted constant diffusion, as expected for an *in vitro* preparation (Foster et al. 2005, Galeffi et al. 2011). The base line pO2 within the CA1 region was similar in both age groups (P5: 163 ± 27 mm Hg; P7: 112 ± 25 mm Hg; p=0.3) indicating that the experimental conditions provided sufficient oxygen in the CA1 region, always above the critical hypoxia threshold of 7.5 mm Hg (Erecinska and Silver 2001, Kasischke et al. 2011). At P5, there was a consistent, net oxygen decrease and NADH rise with each ILE (Fig. 4 P5 panel lower trace; NADH, red trace), coincident with ILE onset, indicating a marked increased oxygen utilization within the tissue during each ILE (82 ± 4 mm Hg, n = 20, see also Fig. 5 E). At the end of each ILE, when NADH reached its maximum, the oxygen slowly returned to baseline levels (Fig. 4 P5, P7 insets). However, with later ILE occurrences at P5 the baseline oxygen tension between ILEs declined slightly, suggesting less than complete recovery from each ictal event (i.e., continued enhanced oxygen utilization) and/or more intense interictal activity, matching the slow upwards rise of the NADH response (Fig. 1A). *Both the NADH baseline elevation and the progressive baseline decrease in the tissue O2 levels indicate a background increase in metabolism, reflecting both recovery from each ILE event as well as the ongoing epileptiform hyperactivity*.

Figure 4 (P7 panel) shows the relative amplitude of the oxygen dip with the initial ILE in low-Mg2+ condition at P7, with a small, initial decline in the baseline oxygen level (prior to the occurrence of the first ILE), concurrent with a small, negative DC offset (Fig. 4 P7). The oxygen dip persisted longer with each ILE at P7 as compared to P5, indicating a more prolonged period of increased oxygen utilization at P7. Further, the LFP base line did not entirely recover after each ILE (see also Fig. 3), eventually leading to a notable negative DC shift at the onset of LRDs. Additionally, after the occurrence of the last ILE and during the transition into LRDs, there was a pronounced, persistent oxygen decrease (residual pO2 was 8-64 mm Hg, N=5) suggesting a high level of ongoing metabolism during the LRD events, concurrent with the large rise in NADH (Fig. 3). The pO2 increased slightly after reverting to regular aCSF (by 32 ± 8 mm Hg, N=5) but did not recover to the initial level, confirming that the metabolic oxygen utilization declined slightly with the change back to normal medium, and that the tissue could still respond to the change in Mg2+ levels. Note that the tissue oxygen response stays well above zero at both P5 and P7 with a rapid rebound during

the ILE occurrences, again indicating sufficient oxygen flux into the tissue so that there is no hypoxia at any point throughout this epileptiform process (Foster et al. 2005, Galeffi et al. 2011). *The tissue O2 levels clarify the significant, ongoing metabolic requirements associated with the hyperexcitability, and the elevated NADH baseline, indicating a persistent, high level of metabolic activity*.

Comparison of NADH and O2 Transients at P5 and P7

Figure 5A shows the oxygen depth profile under baseline conditions at both P5 and P7, slowly advancing the oxygen electrode progressively deeper into the tissue, beginning at the CA1 ventricular surface. In spite of the high aCSF flow rate there is a rapid falloff within the tissue, to nearly zero at a depth of 300 μm, similar to submerged (Hajos et al. 2009) but not interface (Foster et al. 2005) brain slices. At this stage of development, the thickness of the CA1 area (i.e., from the alveus to the hippocampal fissure) is ∼ 150 μm. Thus, the CA1 region is well oxygenated (i.e., above 100 mm Hg at baseline; Fig. 5A framed points). pO2 depth profiles are similar at both ages, indicating that the experimental conditions provide an equivalent oxygenation of the intact hippocampi at P5 as well as at P7. This profile is similar to submerged adult tissue slices (Hajos et al. 2009) and organotypic hippocampal cultures (Heinemann et al. 2002, Kovacs et al. 2002) but different than interface tissue slices (Foster et al. 2005), which show a U-shaped profile since there is oxygen-rich media below the slice as well as a high concentration of oxygen at the upper slice surface.

Fig. 5B shows a comparison of ILE durations across the two age groups, indicating a wide range of ILE length in both conditions. Two sample t-test did not reveal any age related difference in ILE durations (56 ± 2 s at P5 vs 57 ± 2 s at P7; p=0.72, n=32). Figure 5C shows typical averaged (black) NADH responses during ILE events for P5 (left) and P7 (right), as well as the variability of individual responses (gray). The amplitude of the initial NADH decrease was larger at P5-6 than at P7 (-0.77 ± 0.07 % vs -0.4 ± 0.05 %, $p<0.0001$, $n>24$, Figure 5D). The amplitudes of the NADH increase phases were similar (5.59 ± 0.25 % at P5, vs 6.29 ± 0.46 %; p= 0.09, n>24, Figure 5). Although there was no difference in ILE duration, the amplitude of the oxygen transient associated with ILEs was larger at P7 than at P5-6 (119 ± 6 mm Hg vs 82 ± 4 mm Hg; $p<0.0001$, $n>14$) suggesting a higher oxygen consumption probably due to the more intense neuronal activity and synchrony during ILE generated at P7, probably reflecting the maturation of the hippocampal circuitry (Fig. 5E).

FAD+ and tissue oxygen recording confirm enhanced metabolism during ILEs and LRDs

Since NADH fluorescence imaging can differ from oxygen utilization and oxidative phosphorylation, and to also differentiate metabolic NADH from NADPH (Galeffi et al, 2011), we wanted to assess mitochondrial contribution also measuring FAD+, which mediates electron transport at complex II within mitochondria. In contrast to NADH, which has similar spectral properties to NADPH, but which is less metabolically active, FAD+ relates directly to oxidative phosphorylation (Huchzermeyer et al. 2008, Zhao et al. 2011). In several recent reports the NADH and FAD+ responses to synaptic trains were nearly symmetric (Shuttleworth 2010, Ivanov et al. 2014) whereas in another report there were clear differences in waveform shape between NADH and FAD+ (Rosner et al. 2013).

Further, a recent report showed differences in metabolic responses between NADH and NADPH, when separated using different time responses during NADH lifetime imaging, indicating that the NADPH component was minimally metabolically active on a short time scale (Blacker et al. 2014). Thus, the major aspect of the metabolically active NAD(P)H responses on a rapid time scale (ie, seconds) clearly is attributable to NADH, whereas NADPH shows less metabolic involvement and is subtracted out using our difference imaging approach. Hence, we designate our metabolic imaging responses to primarily NADH (Shuttleworth 2010).

We combined FAD+ imaging and tissue oxygen measurements at both P5/P6 and P7 (Fig. 6; n = 4). Note that FAD+ responses are inverted as compared to NADH since the oxidized form of the FAD+/$FADH_2$ pair is the fluorescent chromophore, in contrast to NADH, which is the reduced form of the NAD+/NADH pair. We found a sustained FAD+ decrease (Fig. 6 green traces) with each ILE together with a large oxygen transient response (Fig. 6 blue traces), consistent with and nearly mirroring the NADH responses. At P7 there was an initial decrease associated with the onset of low Mg2+ perfusion (opposite of NADH, where a decrease was noted under some conditions at P5), then a persistent, maintained FAD+ decrease and significant oxygen utilization associated with the onset of LRDs (Fig. 6 P7 panel). These results confirm the presence of a persistently elevated metabolism during LRDs, whilst the activity is of low voltage. FAD+ fluorescence consistently paralleled the pO2 response and independently verified the NADH fluorescence changes, indicating minimal if any role for non-metabolic fluorescence from NADPH.

Metabolic activity associated with bicuculline induced epileptiform activity

Since removal of Mg2+ from the ACSF medium can affect excitatory neurotransmission [ie, enhance NMDA receptor function, possibly at extrasynaptic receptors - (Hardingham et al. 2002)] *and membranes in a non-specific way* (Altura and Altura 1996), *we wished to validate our results using a different "epilepsy" model, i.e. pathological activity induced by the perfusion of bicuculline, a $GABA_A$ receptor antagonist. Since bicuculline is a model of disinhibition there is no direct change in excitatory, glutamatergic synaptic function in the hippocampus. Addition of 10 μM bicuculline to the intact, immature (P7) hippocampus led to IE activity* (Fig. 7) (Cooper et al. 2009). Shortly after starting bicuculline, but prior to occurrence of either ILE or IE events, NADH fluorescence showed a small decrease (-1.6 ± 0.4 %; $p<0.01$, N=6; Fig. 7A arrows), suggesting a diffuse, increased metabolic activity during the initial blockade of inhibition, i.e. a circuitry build-up phase (Cohen et al. 2006). Subsequently, bicuculline led to a rapid rise in NADH fluorescence (0.8 ± 0.2 % per 10 s, N=5) and short ILEs (27 ± 4 s, n=25), IEs, or both. Details are given in Fig. 7B for the short ictal-like events and Fig. 7C for interictal events, comparing the LFP responses with spikes, the NADH responses (with a brief oxidation then reduction) and tissue oxygen levels (showing a transient decrease correlating with the duration of the event).

Figure 7D-F shows the companion FAD+ imaging responses, in comparison to the NADH imaging responses in Fig.'s 7A-C. The FAD+ imaging shows nearly symmetrical metabolic responses, confirming that the majority of the NADH responses are both mitochondrial and

metabolic nature and that any slower, non-metabolic NADPH contribution is effectively subtracted out.

LFP recordings in DC mode showed a small, reversible DC shift during ILEs (-0.25 ± 0.07 mV, p<0.001, n=16). As in low magnesium conditions, the NADH responses to bicuculline-induced ILE started with a decrease (-1.39 ± 0.07 %; n=16, p<0.001) followed by a rapid NADH overshoot (4.65 ± 0.44 %; p<0.001, N=16; Fig. 7B red trace). After ILE offset, high NADH levels persisted, or decreased slowly without returning to initial levels. Metabolic activity during ILEs was confirmed by oxygen consumption: tissue pO2 showed a decrease of 80 ± 6 mm Hg (N=18; Fig. 7B blue trace). When compared to ILEs, IEs were short events (0.64 ± 0.22 s, n=101). However, they produced detectable changes in both NADH fluorescence and tissue oxygen. Each IE was accompanied by a sharp drop in NADH levels (-1.10 ± 0.04 %; p<0.001, n=35) followed by a rise, which could overshoot (0.67 ± 0.07 %; p<0.001; n=35; Fig. 7C red trace). The mean amplitude of the pO2 transient responses was -8.8 ± 0.4 mm Hg (p<0.001, N=35; Fig. 7C blue trace).

Comparison of Metabolic Activity: Bicuculline and Low Mg2+ Conditions

In ten P7 mice, we prepared one hippocampus (called ipsilateral) for perfusion with bicuculline, whilst the other hippocampus (contralateral) was perfused with low magnesium ACSF. Experimental conditions were strictly identical for both treatments, including application time, extracellular electrodes, optical recording configuration, temperature, perfusion rate, aCSF pH and osmolarity. Bicuculline treatment (for > 50 min) never triggered LRDs, in contrast to low Mg2+ ACSF application for 18-45 minutes (31 ± 7 min, N=10). We thus only compared ILE duration, NADH signalling and pO2 changes in first 5 paired experiments (Fig. 8) and FAD signalling in five others. As Fig. 8A shows, the ILEs induced by low Mg2+ were longer than those found in bicuculline (54 ± 5 s vs 34 ± 4 s, respectively; p < 0.001, N =14). The oxygen consumption during these epileptiform events was higher when ILEs were induced by magnesium removal than by $GABA_A$ inhibition: pO2 decrease of -114 ± 6 mm Hg vs -76 ± 6 mm Hg, respectively (p < 0.001, n =14, Fig 8B).

Figure 8C illustrates averaged traces of the NADH transients evoked by low Mg2+ aCSF (left hand side panel, black trace) and bicuculline (grey trace). The only difference is in the amplitude of the initial NADH decrease, which was larger when ILEs were induced by bicuculline than by magnesium removal (-1.54 ± 0.1 % vs -1.03 ± 0.1 %; p < 0.001, n =15). Figure 8D illustrates averaged traces of the FAD transients evoked by low Mg2+ aCSF (left hand side panel, black trace) and bicuculline (grey trace). As in the case of NADH, the oxidative peak of FAD transients (corresponding to NADH oxidative deep) recorded in bicuculline (left hand side panel, grey trace) was significantly larger that observed in low Mg2+ (2.85 ± 0.41 % n=11 vs 0.57 ± 0.20 %, n=8, Fig. 8D, left hand side panel). The reduction phases amplitudes were not significantly different: 7.09 ± 1.23 %, n=8 in low Mg2+ vs 5.45 ± 0.49 %, n=11 in bicuculline (Fig. 8D, left hand side panel). Both NADH and FAD imaging suggest that in bicuculline model of ILE the oxidative phosphorylation at the beginning of epileptiform event has a metabolic rate higher than in low Mg2+.

Interestingly pO2 transients had no difference in decay rate probably due to the sensing capabilities of the oxygen sensing probe.

Discussion

These results establish a taxonomy of metabolic responses during various forms of epilepsy-related activities, comparing two different models of epileptiform events, low Mg2+ and bicuculline. First, there is a robust oxidative metabolic response occurring during each ictal-like event (ILE), revealed by large tissue oxygen decrease (indicating enhanced cellular oxygen utilization) with a combination of a biphasic NADH/FAD responses as expected from previous in vitro and in vivo studies (Pan et al. 2008, Alavi et al. 2011). In general this oxidative response is similar in both low Mg2+ and bicuculline conditions, confirming that it is not just a consequence of the specific type of convulsant. However in bicuculline the NADH/FAD+ oxidative phase is more pronounced than in the low Mg2+ condition, suggesting a higher rate of oxidative phosphorylation at the beginning of each epileptiform event. Second, the late recurrent depolarization occurring in sufficiently mature tissue with low Mg2+ conditions (LRD, at P7) demonstrates a high degree of oxidative metabolism with persistent (and partially reversible) oxygen utilization and increased NADH together with synchronized neuronal activity.

These results confirm our hypothesis that a large difference in metabolism (reflecting circuitry maturation and changes in ionic concentrations, chloride pumps and ligand-gated receptors) occurs between P5 and P7, likely leading to the LRD occurrence at P7 (Wahab et al. 2011). Indeed, at P7, ILEs are of the same duration as at P5 but are accompanied by higher oxygen consumption. Further, the high degree of metabolic activity associated with LRD occurrence indicates this is clearly a form of status epilepticus, similar to non-convulsive status associated with hippocampus in vivo (Sutter and Kaplan 2013). We confirm that LRD activity meets the electroencephalographic criteria for nonconvulsive status epilepticus (Meierkord and Holtkamp 2007, Sutter and Kaplan 2012): duration of abnormal synchronized electrical activity > 5 min and preferably > 30 min (Chen et al. 2007) and an activity pattern consistent with limbic status (Sutter and Kaplan 2012, Sutter and Kaplan 2013), which often includes a persistent low voltage hypersynchrony epileptic pattern. These metabolic changes with LRD also did not lead to spreading depression (Galeffi et al. 2011, Shetty et al. 2014), as ongoing, hyperactive neural activity was still present, confirming our last hypothesis.

Likewise, LRD was not associated with cell death either (Quilichini et al. 2002), as the decreased tissue oxygen levels, physiological function and maintained NADH responses confirmed ongoing cellular metabolism, whereas cell death would elevate tissue oxygen levels (Foster et al. 2005). These results are consistent with those reported in organotypic hippocampal slices (Heinemann et al. 2002, Heinemann et al. 2002) and also acute combined entorhinal-hippocampal slices (Mody et al. 1987, Dreier and Heinemann 1991, Holtkamp et al. 2011). However, we show more robust NADH responses (ie, less decay) than present in organotypic hippocampal tissue slices under low Mg2+ conditions (Kovacs et al. 2002), the clear absence of spreading depression [unlike that predicted by Mody et al (Mody et al. 1987)] and the absence of “metabolic failure” (Heinemann et al. 2002). Thus,

our data extend far beyond previous reports with a more robust preparation (ie, the intact immature hippocampus), the extension of NADH imaging to FAD+ imaging as a comparison, the addition of tissue O2 recordings, all demonstrating a coherent and important metabolic element to epileptiform responses. Though we have analyzed epileptiform activity on immature tissue, the hyperactivity remains similar to that in more mature tissue as well (Mody et al. 1987, Gloveli et al. 1995). A similar metabolic response to ILE generation was also found using another convulsant, 4-aminopyridine (Schuchmann et al. 1999). However, in neocortex picrotoxin was associated with episodes of spreading depression due to K+ dysregulation (Hablitz and Heinemann 1989).

We have demonstrated that imaging NADH and FAD+ metabolic fluorescence in intact, immature hippocampi correlates well with electrophysiological epileptiform activity and that together NADH and FAD+ fluorescence and oxygen recordings confirm the high metabolic demand associated with the epileptiform events. A net NADH oxidation preceded overt epileptiform activity with both bicuculline and low Mg2+ conditions (O'Connor et al. 1972), suggesting that circuitry build-up upon initiation of hyperexcitable conditions leads to intense metabolic activity, mainly glycolytic since the activity was not associated with significant (detectable) oxygen utilization and FAD rise at this early stage. However, both interictal and ILE responses demonstrate an intense metabolic demand, as indicated by the combination of NADH/FAD changes together with decreased tissue oxygen, associated with enhanced neuronal synchrony. The NADH imaging technique can also resolve timing in coordination with the physiology, for example the NADH oxidation preceding overt ILE occurrence (O'Connor et al. 1972, Schuchmann et al. 1999, Heinemann et al. 2002, Kann et al. 2005). However, NADH imaging does not have sufficient time resolution for imaging seizure spread, since metabolic events require seconds for development; to achieve improved time resolution, voltage sensitive dyes and faster imaging techniques are required (Derchansky et al. 2006, Kibler and Durand 2011, Ma et al. 2013).

These simultaneous electrophysiological and NADH fluorescence results in low-Mg2+ epileptiform conditions are consistent with previous reports using NADH or other metabolic imaging in mature hippocampal-entorhinal slices and slice cultures, where brief SLEs (duration ~ 20-40 sec) occur spontaneously (Heinemann et al. 2002, Heinemann et al. 2002). Although NADH imaging in mature combined slices revealed a patterned decrease/increase with each SLE similar to that noted in immature tissue, a pattern of fatigue was also noted over time, with eventually decreased fade in the NADH response (note Fig. 1, Heinemann et al. 2002b) (Heinemann et al. 2002). *In contrast, we found a progressive elevation of the NADH baseline, which may due to the different preparations and their relative metabolic conditions (severed tissue for slices vs an intact structure as used here), whereas in organotypic slices Kovacs et al reported a "rundown" of NADH responses, particularly after ~15 ILE events* (Kovacs et al. 2002).

The FAD+ responses are similar to those recorded in neocortex with epileptiform events (but referred to as "AFI" in that paper (Zhao et al. 2011) and also during spontaneous network activity at different oxygen concentrations (Huchzermeyer et al. 2008). During a 4-AP seizure (lasting ~ 60 sec with a single, monophasic field potential) induced in intact neocortex the focus showed an initial FAD+ oxidation then after 2-5 sec a switch to

reduction (Zhao et al. 2011); the complex surround area showed opposite effects. We observed minimal initial FAD+ oxidation (small even in the NADH imaging) in low Mg2+ conditions but this oxidation was very pronounced in bicuculline. However, the oxygen levels and responsiveness are very different in intact, *in vivo* cortex as compared to *in vitro* preparations, which may distort the NADH/FAD+ waveforms (Turner et al. 2007, Galeffi et al. 2011). The overall correlation between the NADH fluorescence and the integrated field potential (obtained solely from CA1) strongly suggests that the intact hippocampal CA1 region remains viable during these epileptiform conditions, however, arguing against any damaging "hypoxia" resulting from the limited oxygen availability. This viability in CA1 is further reinforced by the oxygen profile data (Fig. 5A) confirming the suitable, physiological oxygen levels at baseline within the more superficial CA1 region.

Several physiological events in hippocampus lead to measurable NADH responses, including physiological train stimulation (Galeffi et al. 2007, Galeffi et al. 2011), epileptiform events (Heinemann et al. 2002), and spreading depression (Foster et al. 2005, Galeffi et al. 2011). In moderate physiological train stimulation (at 10 Hz) under well-oxygenated conditions, for example, the NADH response demonstrates a maintained oxidation for the duration of the train, similar to NADH responses recorded *in vivo* (Galeffi et al. 2011). However, if the oxygen level is reduced so oxygen availability is restricted then the NADH biphasic response emerges in response to an identical train, with an initial, brief oxidation followed by a prolonged reduction. Thus, the morphology of the NADH responses to metabolic activation can vary depending upon relative oxygen availability in the absence of hypoxia (Erecinska and Silver 2001, Galeffi et al. 2011, Kasischke et al. 2011). Another source of mismatch can be high metabolic demand even in readily available oxygen conditions, as is the case with spreading depression, where the NADH oxidation is curtailed and a prolonged, heightened reduction rapidly follows (Galeffi et al. 2011). Thus, the NADH response can be misleading if there is a mismatch between oxygen supply and demand, particularly under *in vitro* conditions where oxygen supply is usually limited by diffusion as in this intact hippocampus preparation. *Overall, the NADH/FAD+ responses together with the tissue oxygen measurements confirm primarily oxidative metabolism during IEs, though it may difficult to distinguish an NADH cytosolic component to the responses* (McKenna et al. 2006, Galeffi et al. 2007).

Ictal and interictal like activities induced by bicuculline do not typically lead to a prolonged or irreversible condition as noted with low Mg2+-induced LRD (Mody et al. 1987, Gloveli et al. 1995, Quilichini et al. 2002). The LRD condition begins during low Mg2+ conditions and persists even after removal of the epileptogenic condition, when normal Mg2+ concentration (1.3 mM) is restored. This means that persistent LRD activity after return to normal Mg2+ levels is no longer sustained by an external factor so LRDs reflect the intrinsic property of the hippocampal network, after being modified by the low Mg2+ condition and ILE generation. Thus, at P7 the low Mg2+ condition (in contrast to bicuculline-induced ILEs) irreversibly modifies neuronal and/or astrocytic functioning (Quilichini et al. 2002, Quilichini et al. 2003). This suggests that molecular pathways activated during ILE in bicuculline are not the same as in the case of low Mg2+.

With NADH/FAD imaging we revealed at least one difference in the intracelluar signalling associated with low Mg2+ versus bicuculline conditions: the rapid oxidation of FAD+/NADH at the beginning of ILE is either low amplitude or non-existent in low Mg2+ but is always present and has significantly higher amplitude in bicuculline. This indicates a higher rate of mitochondrial oxidative phosphorylation during bicuculline compared to low Mg2+ - induced ILEs, possibly due to different forms of hypersynchrony and differences in Ca2+ entry (Griffiths and Rutter 2009). Decreased magnesium enhances the sensitivity of NMDA receptors to the ambient glutamate at resting membrane potentials, which stimulates calcium entry mainly through NR2B/NR2D - containing extrasynaptic NMDARs, because they have a higher affinity to the neurotransmitter and are more permeable for Ca2+ then synaptic NR2A- containing receptors (Erreger et al. 2007). In contrast, the network disinhibition with bicuculline increases synaptic activity and therefore stimulatesCa2+ entry, mainly through synaptic NMDARs (Ivanov et al. 2006). Synaptic and extrasynaptic NMDARs lead to opposing actions on intracellular signalling pathways and activate distinct genomic programs (Hardingham and Bading 2010). Therefore, the extrasynaptic calcium entry induced by magnesium removal may modify mitochondrial metabolism in a manner separate from synaptic calcium entry during bicuculline application, which could differentially modify neuronal properties and enhance network susceptibility to the generation of LRDs.

NADH persisted as an increase throughout the LRD phase (Fig. 3A) while oxygen remained depressed below the initial level (Fig. 4 P7). This confirms that direct pO2 measurement can provide a better estimate of overall network activity than LFP alone: the tightly synchronized, low voltage neuronal activity during the LRD phase may be superficially interpreted as less intense physiologically, as compared to ILE occurrences, or a tissue fatigue response (Galeffi et al. 2011). Indeed, when compared with ILEs the LRD event seems to only consist of low amplitude fluctuations therefore the associated high energy consumption is rather unexpected.

However, as shown in Figs. 3 LRDs are accompanied by a DC offset that could be indicative of the massive depolarization and extracellular potassium increase associated with low Mg2+ conditions (Gloveli et al. 1995, Heinemann et al. 2002). *However, the maintained physiological and metabolic activity precludes a spreading depression occurrence* (Mody et al. 1987, Gloveli et al. 1995), *unlike which occurs in neocortex in a different hyperexcitability model, picrotoxin* (Hablitz and Heinemann 1989). *Certainly in the LRD condition energy dependent mechanisms such as ionic pumps and exchangers are activated to maintain physiological membrane potential* (Schuchmann et al. 1999). *Interestingly, the transition into the LRD state was not observed at P5, consistent with previous reports in rat isolated hippocampi* (Quilichini et al. 2002, Quilichini et al. 2003), *possibly due to further developmental maturation of hippocampal circuitry by P7* (Wahab et al. 2011).

If ILEs were maintained (as in the P7 experiments – Fig. 3) then this persistent high metabolic activity would likely create an energy deficit, possibly leading to neuronal and tissue damage, as measured by Heinemann et al in organotypic hippocampal slices exposed to low Mg2+ (Heinemann et al. 2002, Heinemann et al. 2002). Clearly, the LRD condition demonstrates a high metabolic demand due to the persistently lowered oxygen and maintained NADH/FAD+ reduction, indicating that this condition is similar to

nonconvulsive status epilepticus, as suggestive by multiple reports (Dreier and Heinemann 1991, Heinemann et al. 2002, Holtkamp et al. 2011). The persistent LRD state is also similar in duration and electrical morphology to nonconvulsive status epilepticus (though of course without the behavioural consequences) (Wasterlain et al. 1993, Chen et al. 2007, Meierkord and Holtkamp 2007, Sutter and Kaplan 2012). Even *in vivo* under intact conditions persistent seizure behaviour may lead to an accumulating metabolic deficit and tissue damage due to paralysis of neurovascular coupling, the frequent ultimate outcome of status epilepticus (Duffy et al. 1975, Chapman et al. 1977, Folbergrova et al. 1981, Zilberter et al. 2010, Sutter and Kaplan 2012). Whether this deficit contributes to the postictal state remains an intriguing question, since it is not clear if seizures stop solely due to build-up of ionic shifts (Krishnan and Bazhenov 2011) or due to tissue metabolic exhaustion (Theodore 2010).

Diagnosis and treatment of epilepsy has often involved metabolic approaches. In most *in vivo* studies of seizures neurovascular coupling correspondingly leads to enhanced substrate to at least theoretically match the heightened metabolism required for seizures, though the postictal state may represent “exhaustion” to a point (Theodore 2010, Zhao et al. 2011). Cell damage with status epilepticus could arise following depletion of critical energy substrates (Duffy et al. 1975, Chapman et al. 1977). Further, several metabolic approaches have been clinically used for seizure treatment and prevention, with an interest in ketogenic diet and use of 2-DG to partially block glycolysis and hence reduce epileptic threshold (Stafstrom et al. 2008, Milder and Patel 2012)). For example, the ketogenic diet has several possible metabolic mechanisms, including changes in the relative balance of aerobic glycolysis and oxidative metabolism due to the relative hypoglycemia which occurs in this diet. Additionally, both iodoacetate *in vivo* and 2-DG partially block glycolysis in a direct manner (Dora 1983).

In summary, the density of synchronized, epileptiform activity can be discriminated on the basis of metabolic demand, with low-Mg2+ induced ILEs showing less oxidative metabolism than the long-lasting LRD condition, demonstrating a continuous high metabolism and constant seizure state associated with persistently high oxygen demand. The tissue oxygen recordings substantially enhance the NADH/FAD+ fluorescence measurements in metabolic analysis. The intact hippocampus, in spite of its immature developmental stage, encompasses sufficient circuitry for the full development of spontaneous seizure-like events and status epilepticus, as compared to tissue slices of hippocampus alone, hence provides an adequate substrate for analysis of critical factors underlying epileptiform activity (Schwartzkroin 1986).

Acknowledgments

This research was supported by INSERM UMR1106 (AI, CB), NIH Senior Fellowship NIH F33 NS062617 (DAT, CB), NIH R01 NS051856 (DAT), and NIH R01AG037599 (DAT).

References

Alavi A, Yakir S, Newberg AB. Positron emission tomography in seizure disorders. Annals of the New York Academy of Sciences. 2011; 1228:E1–E12. [PubMed: 22239278]

Altura BM, Altura BT. Role of magnesium in patho-physiological processes and the clinical utility of magnesium ion selective electrodes. Scandinavian journal of clinical and laboratory investigation. Supplementum. 1996; 224:211–234. [PubMed: 8865438]

Aubin JE. Autofluorescence of viable cultured mammalian cells. The journal of histochemistry and cytochemistry : official journal of the Histochemistry Society. 1979; 27(1):36–43. [PubMed: 220325]

Blacker TS, Mann ZF, Gale JE, Ziegler M, Bain AJ, Szabadkai G, Duchen MR. Separating NADH and NADPH fluorescence in live cells and tissues using FLIM. Nature communications. 2014; 5:3936.

Chapman AG, Meldrum BS, Siesjo BK. Cerebral metabolic changes during prolonged epileptic seizures in rats. Journal of neurochemistry. 1977; 28(5):1025–1035. [PubMed: 16986]

Chen JW, Naylor DE, Wasterlain CG. Advances in the pathophysiology of status epilepticus. Acta neurologica Scandinavica. Supplementum. 2007; 186:7–15. [PubMed: 17784531]

Cohen I, Huberfeld G, Miles R. Emergence of disinhibition-induced synchrony in the CA3 region of the guinea pig hippocampus in vitro. The Journal of physiology. 2006; 570(Pt 3):583–594. [PubMed: 16322056]

Cooper CE, Cope M, Elwell CE, Delpy DT. Bicuculline-induced seizures: a challenge for optical and biochemical modeling of the cytochrome oxidase CuA NIRS signal. Advances in experimental medicine and biology. 2009; 645:129–134. [PubMed: 19227461]

Derchansky M, Rokni D, Rick JT, Wennberg R, Bardakjian BL, Zhang L, Yarom Y, Carlen PL. Bidirectional multisite seizure propagation in the intact isolated hippocampus: the multifocality of the seizure “focus”. Neurobiology of disease. 2006; 23(2):312–328. [PubMed: 16815026]

Derchansky M, Shahar E, Wennberg RA, Samoilova M, Jahromi SS, Abdelmalik PA, Zhang L, Carlen PL. Model of frequent, recurrent, and spontaneous seizures in the intact mouse hippocampus. Hippocampus. 2004; 14(8):935–947. [PubMed: 15390177]

Dora E. Glycolysis and epilepsy-induced changes in cerebrocortical NAD/NADH redox state. Journal of neurochemistry. 1983; 41(6):1774–1777. [PubMed: 6644311]

Dreier JP, Heinemann U. Regional and time dependent variations of low Mg2+ induced epileptiform activity in rat temporal cortex slices. Experimental brain research. 1991; 87(3):581–596. [PubMed: 1783028]

Duffy TE, Howse DC, Plum F. Cerebral energy metabolism during experimental status epilepticus. Journal of neurochemistry. 1975; 24(5):925–934. [PubMed: 237981]

Dzhala VI, Brumback AC, Staley KJ. Bumetanide enhances phenobarbital efficacy in a neonatal seizure model. Annals of neurology. 2008; 63(2):222–235. [PubMed: 17918265]

Dzhala VI, Kuchibhotla KV, Glykys JC, Kahle KT, Swiercz WB, Feng G, Kuner T, Augustine GJ, Bacskai BJ, Staley KJ. Progressive NKCC1-dependent neuronal chloride accumulation during neonatal seizures. The Journal of neuroscience : the official journal of the Society for Neuroscience. 2010; 30(35):11745–11761. [PubMed: 20810895]

Erecinska M, Silver IA. Tissue oxygen tension and brain sensitivity to hypoxia. Respiration physiology. 2001; 128(3):263–276. [PubMed: 11718758]

Erreger K, Geballe MT, Kristensen A, Chen PE, Hansen KB, Lee CJ, Yuan H, Le P, Lyuboslavsky PN, Micale N, Jorgensen L, Clausen RP, Wyllie DJ, Snyder JP, Traynelis SF. Subunit-specific agonist activity at NR2A-, NR2B-, NR2C-, and NR2D-containing N-methyl-D-aspartate glutamate receptors. Molecular pharmacology. 2007; 72(4):907–920. [PubMed: 17622578]

Folbergrova J, Ingvar M, Nevander G, Siesjo BK. Cerebral metabolic changes during and following fluorothyl-induced seizures in ventilated rats. Journal of neurochemistry. 1985; 44(5):1419–1426. [PubMed: 3989540]

Folbergrova J, Ingvar M, Siesjo BK. Metabolic changes in cerebral cortex, hippocampus, and cerebellum during sustained bicuculline-induced seizures. Journal of neurochemistry. 1981; 37(5): 1228–1238. [PubMed: 7299397]

Foster KA, Beaver CJ, Turner DA. Interaction between tissue oxygen tension and NADH imaging during synaptic stimulation and hypoxia in rat hippocampal slices. Neuroscience. 2005; 132(3): 645–657. [PubMed: 15837126]

Foster KA, Galeffi F, Gerich FJ, Turner DA, Muller M. Optical and pharmacological tools to investigate the role of mitochondria during oxidative stress and neurodegeneration. Progress in neurobiology. 2006; 79(3):136–171. [PubMed: 16920246]

Galeffi F, Foster KA, Sadgrove MP, Beaver CJ, Turner DA. Lactate uptake contributes to the NAD(P)H biphasic response and tissue oxygen response during synaptic stimulation in area CA1 of rat hippocampal slices. Journal of neurochemistry. 2007; 103(6):2449–2461. [PubMed: 17931363]

Galeffi F, Somjen GG, Foster KA, Turner DA. Simultaneous monitoring of tissue PO2 and NADH fluorescence during synaptic stimulation and spreading depression reveals a transient dissociation between oxygen utilization and mitochondrial redox state in rat hippocampal slices. Journal of cerebral blood flow and metabolism : official journal of the International Society of Cerebral Blood Flow and Metabolism. 2011; 31(2):626–639.

Gloveli T, Albrecht D, Heinemann U. Properties of low Mg2+ induced epileptiform activity in rat hippocampal and entorhinal cortex slices during adolescence. Brain research Developmental brain research. 1995; 87(2):145–152. [PubMed: 7586496]

Griffiths EJ, Rutter GA. Mitochondrial calcium as a key regulator of mitochondrial ATP production in mammalian cells. Biochimica et biophysica acta. 2009; 1787(11):1324–1333. [PubMed: 19366607]

Hablitz JJ, Heinemann U. Alterations in the microenvironment during spreading depression associated with epileptiform activity in the immature neocortex. Brain research Developmental brain research. 1989; 46(2):243–252. [PubMed: 2720957]

Hajos N, Ellender TJ, Zemankovics R, Mann EO, Exley R, Cragg SJ, Freund TF, Paulsen O. Maintaining network activity in submerged hippocampal slices: importance of oxygen supply. The European journal of neuroscience. 2009; 29(2):319–327. [PubMed: 19200237]

Hardingham GE, Fukunaga Y, Bading H. Extrasynaptic NMDARs oppose synaptic NMDARs by triggering CREB shut-off and cell death pathways. Nature neuroscience. 2002; 5(5):405–414.

Heinemann U, Buchheim K, Gabriel S, Kann O, Kovacs R, Schuchmann S. Cell death and metabolic activity during epileptiform discharges and status epilepticus in the hippocampus. Progress in brain research. 2002; 135:197–210. [PubMed: 12143341]

Heinemann U, Buchheim K, Gabriel S, Kann O, Kovacs R, Schuchmann S. Coupling of electrical and metabolic activity during epileptiform discharges. Epilepsia. 2002; 43(Suppl 5):168–173. [PubMed: 12121315]

Holtkamp M, Buchheim K, Elsner M, Matzen J, Weissinger F, Meierkord H. Status epilepticus induces increasing neuronal excitability and hypersynchrony as revealed by optical imaging. Neurobiology of disease. 2011; 43(1):220–227. [PubMed: 21440625]

Huchzermeyer C, Albus K, Gabriel HJ, Otahal J, Taubenberger N, Heinemann U, Kovacs R, Kann O. Gamma oscillations and spontaneous network activity in the hippocampus are highly sensitive to decreases in pO2 and concomitant changes in mitochondrial redox state. The Journal of neuroscience : the official journal of the Society for Neuroscience. 2008; 28(5):1153–1162. [PubMed: 18234893]

Ivanov A, Pellegrino C, Rama S, Dumalska I, Salyha Y, Ben-Ari Y, Medina I. Opposing role of synaptic and extrasynaptic NMDA receptors in regulation of the extracellular signal-regulated kinases (ERK) activity in cultured rat hippocampal neurons. The Journal of physiology. 2006; 572(Pt 3):789–798. [PubMed: 16513670]

Ivanov AI, Malkov AE, Waseem T, Mukhtarov M, Buldakova S, Gubkina O, Zilberter M, Zilberter Y. Glycolysis and oxidative phosphorylation in neurons and astrocytes during network activity in hippocampal slices. Journal of cerebral blood flow and metabolism : official journal of the International Society of Cerebral Blood Flow and Metabolism. 2014; 34(3):397–407.

Jirsa VK, Stacey WC, Quilichini PP, Ivanov AI, Bernard C. On the nature of seizure dynamics. Brain : a journal of neurology. 2014

Kann O, Kovacs R, Njunting M, Behrens CJ, Otahal J, Lehmann TN, Gabriel S, Heinemann U. Metabolic dysfunction during neuronal activation in the ex vivo hippocampus from chronic epileptic rats and humans. Brain : a journal of neurology. 2005; 128(10):2396–2407. [PubMed: 15958506]

Kasischke KA, Lambert EM, Panepento B, Sun A, Gelbard HA, Burgess RW, Foster TH, Nedergaard M. Two-photon NADH imaging exposes boundaries of oxygen diffusion in cortical vascular supply regions. Journal of cerebral blood flow and metabolism : official journal of the International Society of Cerebral Blood Flow and Metabolism. 2011; 31(1):68–81.

Kibler AB, Durand DM. Orthogonal wave propagation of epileptiform activity in the planar mouse hippocampus in vitro. Epilepsia. 2011; 52(9):1590–1600. [PubMed: 21668440]

Kovacs R, Schuchmann S, Gabriel S, Kann O, Kardos J, Heinemann U. Free radical-mediated cell damage after experimental status epilepticus in hippocampal slice cultures. Journal of neurophysiology. 2002; 88(6):2909–2918. [PubMed: 12466417]

Kovacs R, Schuchmann S, Gabriel S, Kardos J, Heinemann U. Ca2+ signalling and changes of mitochondrial function during low-Mg2+-induced epileptiform activity in organotypic hippocampal slice cultures. The European journal of neuroscience. 2001; 13(7):1311–1319. [PubMed: 11298791]

Kreisman NR, Lamanna JC, Rosenthal M, Sick TJ. Oxidative metabolic responses with recurrent seizures in rat cerebral cortex: role of systemic factors. Brain research. 1981; 218(1-2):175–188. [PubMed: 6268244]

Kreisman NR, Sick TJ, Rosenthal M. Importance of vascular responses in determining cortical oxygenation during recurrent paroxysmal events of varying duration and frequency of repetition. Journal of cerebral blood flow and metabolism : official journal of the International Society of Cerebral Blood Flow and Metabolism. 1983; 3(3):330–338.

Krishnan GP, Bazhenov M. Ionic dynamics mediate spontaneous termination of seizures and postictal depression state. The Journal of neuroscience : the official journal of the Society for Neuroscience. 2011; 31(24):8870–8882. [PubMed: 21677171]

Ma H, Zhao M, Schwartz TH. Dynamic neurovascular coupling and uncoupling during ictal onset, propagation, and termination revealed by simultaneous in vivo optical imaging of neural activity and local blood volume. Cerebral cortex (New York, NY : 1991). 2013; 23(4):885–899.

McKenna MC, Waagepetersen HS, Schousboe A, Sonnewald U. Neuronal and astrocytic shuttle mechanisms for cytosolic-mitochondrial transfer of reducing equivalents: current evidence and pharmacological tools. Biochemical pharmacology. 2006; 71(4):399–407. [PubMed: 16368075]

Meierkord H, Holtkamp M. Non-convulsive status epilepticus in adults: clinical forms and treatment. Lancet neurology. 2007; 6(4):329–339.

Milder J, Patel M. Modulation of oxidative stress and mitochondrial function by the ketogenic diet. Epilepsy research. 2012; 100(3):295–303. [PubMed: 22078747]

Mody I, Lambert JD, Heinemann U. Low extracellular magnesium induces epileptiform activity and spreading depression in rat hippocampal slices. Journal of neurophysiology. 1987; 57(3):869–888. [PubMed: 3031235]

O'Connor MJ, Herman CJ, Rosenthal M, Jobsis FF. Intracellular redox changes preceding onset of epileptiform activity in intact cat hippocampus. Journal of neurophysiology. 1972; 35(4):471–483. [PubMed: 4338564]

Pan JW, Williamson A, Cavus I, Hetherington HP, Zaveri H, Petroff OA, Spencer DD. Neurometabolism in human epilepsy. Epilepsia. 2008; 49(Suppl 3):31–41. [PubMed: 18304254]

Quilichini PP, Diabira D, Chiron C, Ben-Ari Y, Gozlan H. Persistent epileptiform activity induced by low Mg2+ in intact immature brain structures. The European journal of neuroscience. 2002; 16(5): 850–860. [PubMed: 12372021]

Quilichini PP, Diabira D, Chiron C, Milh M, Ben-Ari Y, Gozlan H. Effects of antiepileptic drugs on refractory seizures in the intact immature corticohippocampal formation in vitro. Epilepsia. 2003; 44(11):1365–1374. [PubMed: 14636342]

Quilichini PP, Le Van Quyen M, Ivanov A, Turner DA, Carabalona A, Gozlan H, Esclapez M, Bernard C. Hub GABA neurons mediate gamma-frequency oscillations at ictal-like event onset in the immature hippocampus. Neuron. 2012; 74(1):57–64. [PubMed: 22500630]

Rosner J, Liotta A, Schmitz D, Heinemann U, Kovacs R. A LED-based method for monitoring NAD(P)H and FAD fluorescence in cell cultures and brain slices. Journal of neuroscience methods. 2013; 212(2):222–227. [PubMed: 23142181]

Schuchmann S, Buchheim K, Meierkord H, Heinemann U. A relative energy failure is associated with low-Mg2+ but not with 4-aminopyridine induced seizure-like events in entorhinal cortex. Journal of neurophysiology. 1999; 81(1):399–403. [PubMed: 9914300]

Schwartzkroin PA. Hippocampal slices in experimental and human epilepsy. Advances in neurology. 1986; 44:991–1010. [PubMed: 3706029]

Shetty PK, Galeffi F, Turner DA. Cellular Links between Neuronal Activity and Energy Homeostasis. Frontiers in pharmacology. 2012; 3:43. [PubMed: 22470340]

Shetty PK, Galeffi F, Turner DA. Nicotinamide pre-treatment ameliorates NAD(H) hyperoxidation and improves neuronal function after severe hypoxia. Neurobiology of disease. 2014; 62:469–478. [PubMed: 24184921]

Shuttleworth CW. Use of NAD(P)H and flavoprotein autofluorescence transients to probe neuron and astrocyte responses to synaptic activation. Neurochemistry international. 2010; 56(3):379–386. [PubMed: 20036704]

Stafstrom CE, Roopra A, Sutula TP. Seizure suppression via glycolysis inhibition with 2-deoxy-D-glucose (2DG). Epilepsia. 2008; 49(Suppl 8):97–100. [PubMed: 19049601]

Sutter R, Kaplan PW. Electroencephalographic criteria for nonconvulsive status epilepticus: synopsis and comprehensive survey. Epilepsia. 2012; 53(Suppl 3):1–51. [PubMed: 22862158]

Sutter R, Kaplan PW. The neurophysiologic types of nonconvulsive status epilepticus: EEG patterns of different phenotypes. Epilepsia. 2013; 54(Suppl 6):23–27. [PubMed: 24001065]

Theodore WH. The postictal state: effects of age and underlying brain dysfunction. Epilepsy & behavior : E&B. 2010; 19(2):118–120.

Turner DA, Foster KA, Galeffi F, Somjen GG. Differences in O2 availability resolve the apparent discrepancies in metabolic intrinsic optical signals in vivo and in vitro. Trends in neurosciences. 2007; 30(8):390–398. [PubMed: 17590447]

Wahab A, Albus K, Heinemann U. Age- and region-specific effects of anticonvulsants and bumetanide on 4-aminopyridine-induced seizure-like events in immature rat hippocampal-entorhinal cortex slices. Epilepsia. 2011; 52(1):94–103. [PubMed: 21083847]

Wasterlain CG, Fujikawa DG, Penix L, Sankar R. Pathophysiological mechanisms of brain damage from status epilepticus. Epilepsia. 1993; 34(Suppl 1):S37–53. [PubMed: 8385002]

Zhao M, Nguyen J, Ma H, Nishimura N, Schaffer CB, Schwartz TH. Preictal and ictal neurovascular and metabolic coupling surrounding a seizure focus. The Journal of neuroscience : the official journal of the Society for Neuroscience. 2011; 31(37):13292–13300. [PubMed: 21917812]

Zilberter Y, Zilberter T, Bregestovski P. Neuronal activity in vitro and the in vivo reality: the role of energy homeostasis. Trends in pharmacological sciences. 2010; 31(9):394–401. [PubMed: 20633934]

Abbreviations

NADH	nicotine adenine dinucleotide
FAD+	flavin adenine nucleotide
ILEs	ictal-like events
LRD	late recurrent depolarization
aCSF	artificial cerebrospinal fluid
LFP	local field potential

Highlights

1. Interictal epileptiform activity in P5-P7 hippocampus includes an NADH decrease.
2. Ictal-like activity (ILEs) in low Mg2+ shows a large NADH, oxygen uptake increase.
3. Both low Mg2+ and bicuculline epilepsy models lead to similar ILE metabolic activity.
4. Late, recurrent discharges (LRDs) show persistent, maintained oxidative metabolism.
5. Low voltage LRDs are metabolically consistent with hyperactive status epilepticus.

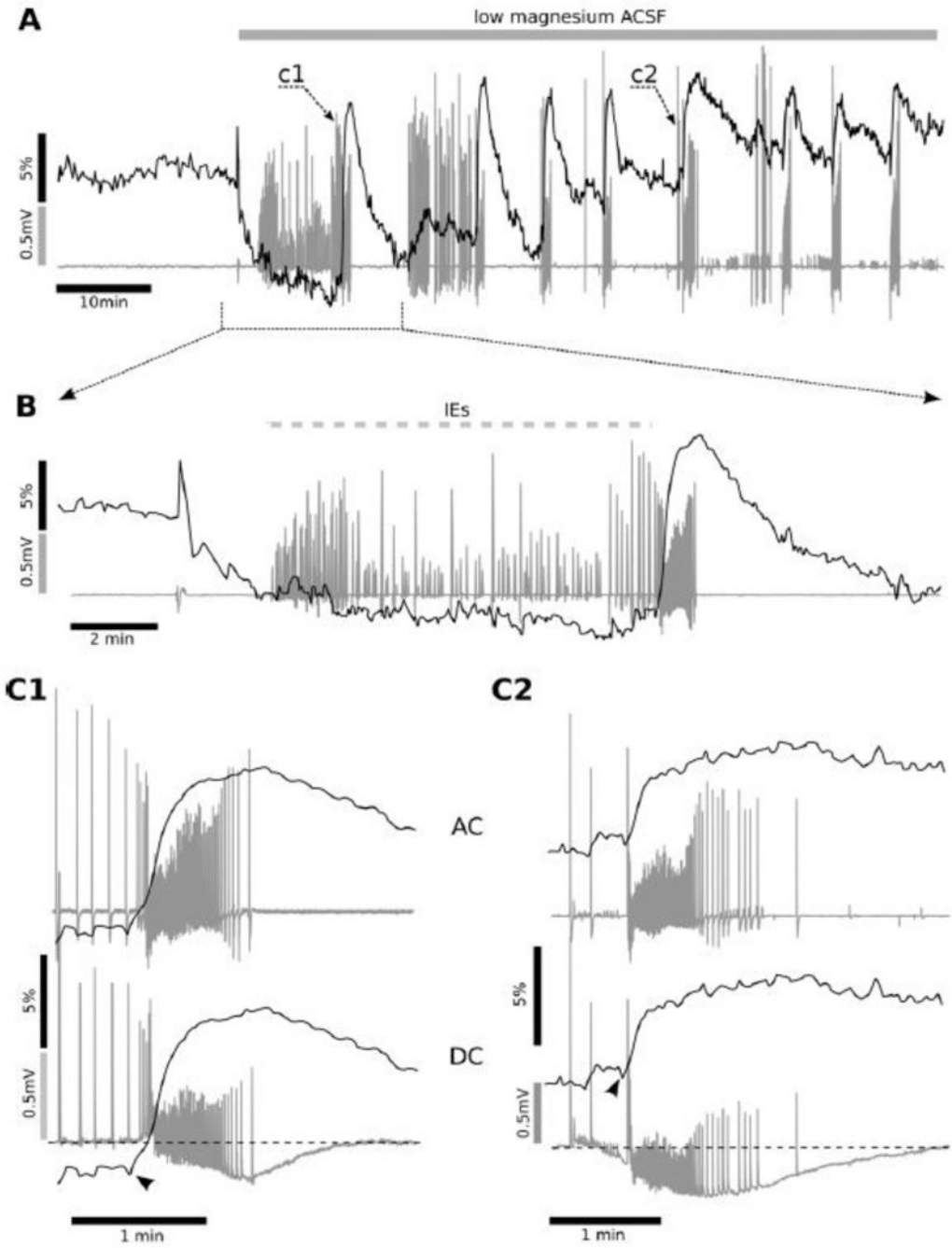

Figure 1. Biphasic NADH changes during interictal- and ictal-like events

Simultaneous recordings of electrical and metabolic activity are shown as overlapping traces. An intact hippocampus from a P5 mouse was perfused with low magnesium aCSF. Magnesium removal first led to a build-up of IE (indicated by a hashed bar) before the onset of the intermittent, spontaneous ictal like discharges (ILEs). The first ILE is shown in c1 (A, grey trace). In B a detail is shown of this build-up period prior to the first ILE, which consists of interictal field potential responses and a slowly decreasing NADH fluorescence level (black trace). Each individual ILE was accompanied by a rapid increase in NADH

fluorescence, usually preceded by a short negative drop in NADH fluorescence (as detailed in C1 and C2 below). ILEs started 6 ± 8 s after the NADH increase onset, which was often preceded by a small NADH decrease (i.e., an oxidation), indicating that the NADH fluorescence signalled the metabolic build-up prior to the overt ILE onset. The NADH rise reached its maximal value and started to decline right after the end of the ILE (C1, C2). The heightened metabolic activity (NADH reduction) persisted during the entire ILE and only slowly declined afterward. Measurements in DC amplifier mode (lower aspects of C1 and C2, grey traces) were performed using an additional extracellular electrode, revealing a negative shift (-0.26 ± 0.8 mV) of the extracellular potential baseline during each ILE. This shift recovered to its initial level within 1-3 min after the end of the ILE.

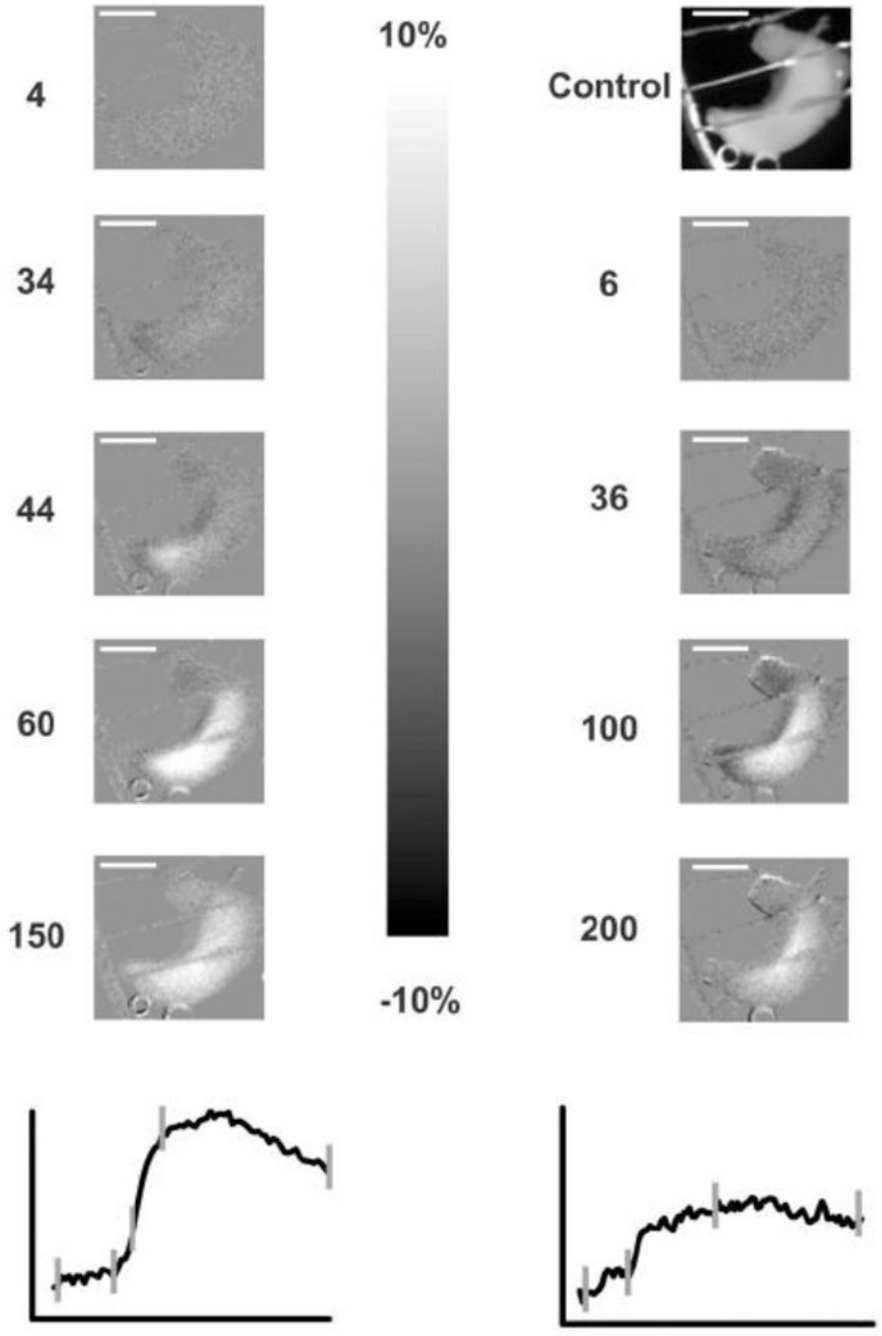

Figure 2. P5 ILE NADH Imaging

This group of NADH fluorescence images show the two ILE's highlighted in Fig. 1 C1 (left) and Fig. 1 C2 (right), with the NADH traces shown below for comparison. The control (unsubtracted) image is shown on the upper right and the other images are shown as normalized images with respect to the control image (i.e., image-control, divided by control). The scale of these subtracted images is +/- 10% from the control image, with lighter values as increased NADH fluorescence and darker as decreased NADH fluorescence. Note the large increases of NADH fluorescence during both ILE occurrences

over time, with the times shown next to the individual images in sec (and shown as vertical hash marks on traces below). The increased NADH signal appears to be uniform over the entire hippocampus except at 44 sec (left) where there is a slight septal preponderance. The scale bars below show 150 ms and 10% difference amplitude vertically. The white scale bar within the images (lower images at 150 and 200 sec) shows 5 mm in the chamber. The NADH time courses were derived from regions of interest in the middle of the hippocampal images.

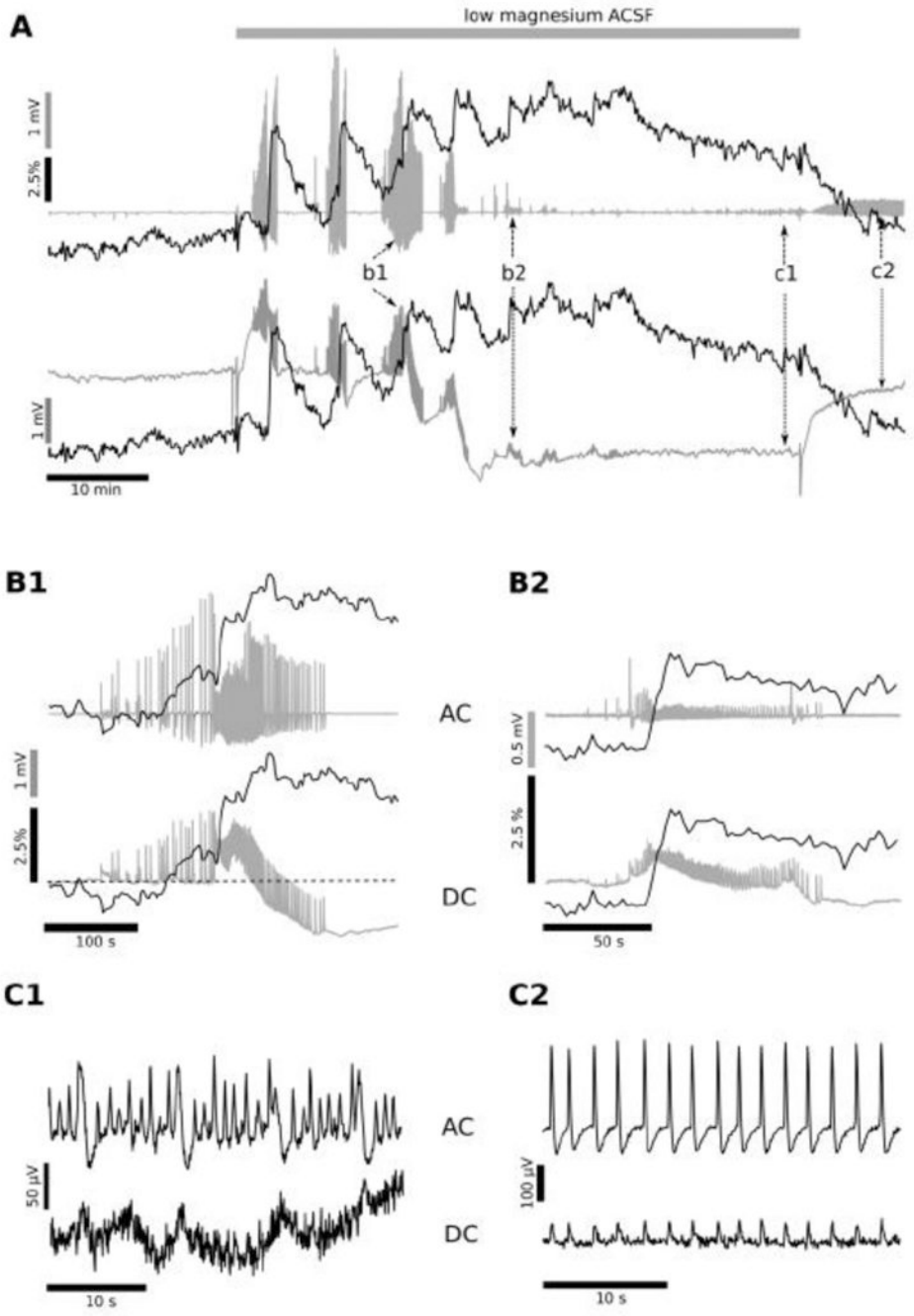

Figure 3. Low Mg2+ condition at P7

Simultaneous recording of the electrical (local field potential, LFP) and metabolic activity (NADH fluorescence) are shown from an intact hippocampus of the P7 mouse in low magnesium aCSF. Experiments conducted on older, P7 mice showed that the application of low Mg2+ aCSF initially induced the generation of 2-5 large amplitude ILEs (A, b1; detail in B1), then progressively the ILEs decreased in amplitude (A, b2; detail in B2), and transformed into low amplitude (50-400 μV) oscillations, with a frequency of 0.6-1.2 Hz (N=7; A, c1; detail in C1). This low amplitude oscillation, late recurrent depolarization

(LRD), persisted even after the switch back to the regular, Mg2+ -containing aCSF (A, c2; detail in C2). Field potential recordings performed in DC mode showed that, similar to experiments in P5 hippocampi, each ILE was accompanied by a baseline negative shift (A, b1, b2: lower trace). The base line behaviour was similar to that observed at P5 during the first 1-2 ILEs (Fig. 1). However, the negative electrical baseline shift grew larger in amplitude (1-3 mV) and irreversible during the last large amplitude ILE (A, b1 lower trace). After this large, negative decrease in the LFP trace the ILE amplitudes decreased (ie, A, b2 as opposed to b1), leading to emergence of LRD behaviour (A, between b2 and c1).

The LFP base line did not completely recover even after the switch to the regular aCSF (between A: c1, c2), continuing 0.5- 1.4 mV more negative that at the beginning of the experiment. The interictal-like events preceding each individual ILE onset were accompanied by a rise in NADH fluorescence (after A, b1), different than the initial, decreased NADH leading up to ILEs in P5 hippocampi (Fig. 1 C1, C2 versus A: c1, c2). The mean amplitude of the NADH fluorescence transient corresponding to the first few ILEs averaged 4.3 ± 1.5% (N=7), but the subsequent ILE transients were smaller in amplitude (B2 vs B1). However, the baseline fluorescence gradually increased over the duration of the exposure to low Mg2+ media, reaching a maximal value of 7.1 ± 2.5% (N=7) at the moment of transition to the LRD generation (A, after b2). Thereafter, the NADH fluorescence remained elevated during the LRD phase (remaining above baseline), and decreased to near the initial value only when the perfusion solution was changed to the regular aCSF (A, after c1). This NADH profile suggests that at P7 the metabolic activity increases not only during each ILE, but also rises prior to ILE occurrence (during the build-up of interictal activity), and continues to increase in the transition to LRD activity, when ILEs are starting to fade. This maintained high NADH level during the transition into LRD activity suggests a profound metabolic demand associated with the ongoing epileptiform activity during this phase.

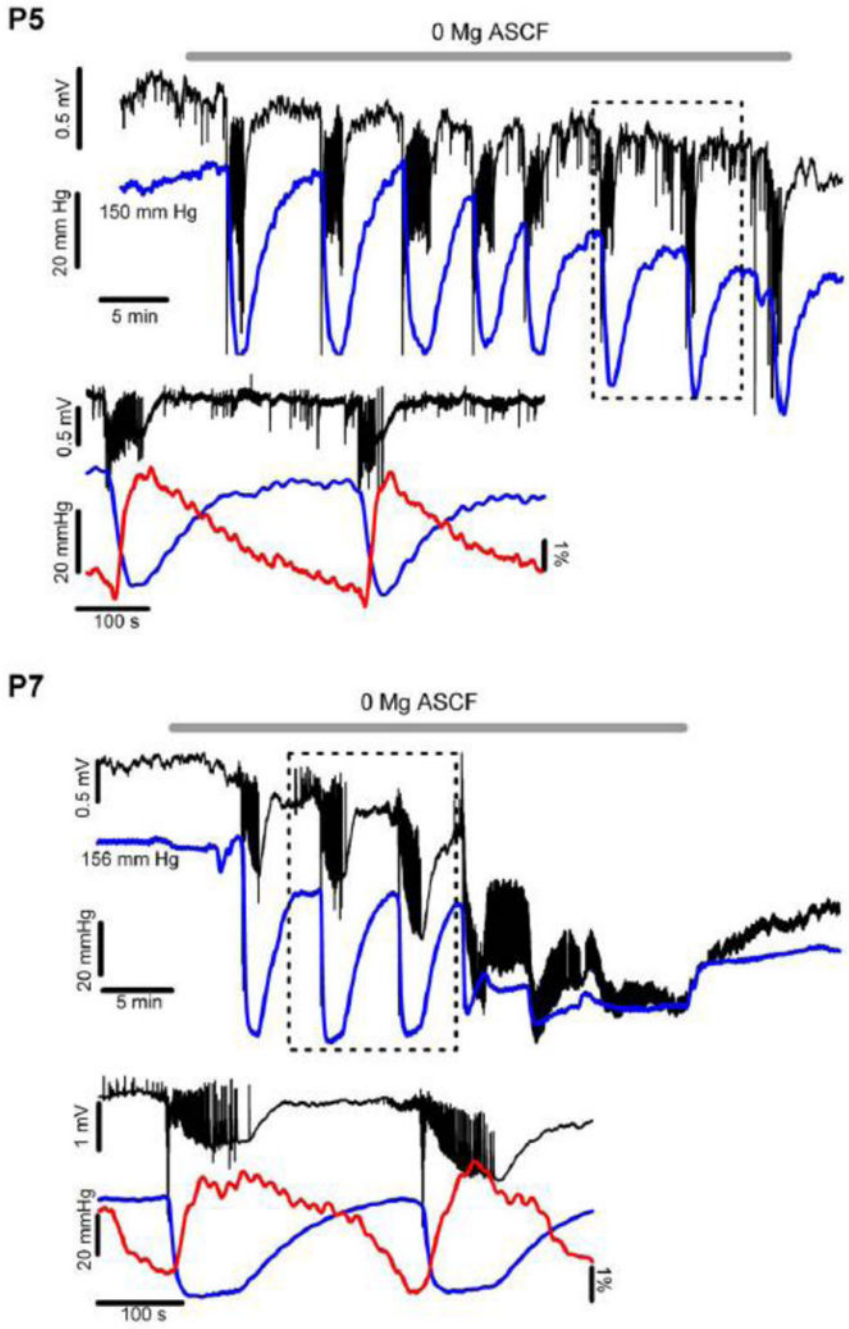

Figure 4. Tissue Oxygen Recordings during P5 and P7 ILEs

These examples demonstrate tissue oxygen levels (blue trace for both P5 [upper panel] and P7 [lower panel]) before and during low Mg2+ aCSF (ambient O2 of 95%). Note that there is an oxygen dip associated with each ILE occurrence, indicating a large, increased metabolic demand during each ILE (lower traces show detail for P5 and P7 panels). Note that the overall oxygen tension baseline declines slightly after multiple ILEs, suggesting an increased overall oxygen debt within the tissue over time. In the P5 experiments the ILE oxygen dip remained nearly constant over the low Mg2+ exposure, averaging near 80 mm

Hg overall (Fig. 5E). In the P7 experiments the oxygen dips associated with each ILE were slightly larger, averaging near 120 mm Hg (Fig. 5E). After several ILE occurrences at P7 the tissue response to the low Mg2+ changed, turning into more diffuse, smaller amplitude and nearly continuous epileptiform spikes (termed LRDs, see also Fig. 3 A, c1 and C1). At this transition the tissue O2 remained at a low level (but still above zero), only slightly increasing even after the low Mg2+ condition was reversed back to normal aCSF, coincident with the ongoing, irreversible LRD activity. This marked increase in tissue O2 utilization suggests considerably increased tissue oxygen demand (and a high metabolic rate) associated with the highly synchronous (but low voltage) LRD events, suggesting nearly continuous epileptiform events. The maintained oxygen utilization during the later phase of P7 experiments correlates well with the heightened NADH levels, both confirming intense metabolic need during the LRD phase. The lower traces for both P5 and P7 show details of the field potential activity, oxygen and NADH, indicating that the oxygen dip coincided with the start of the ILE.

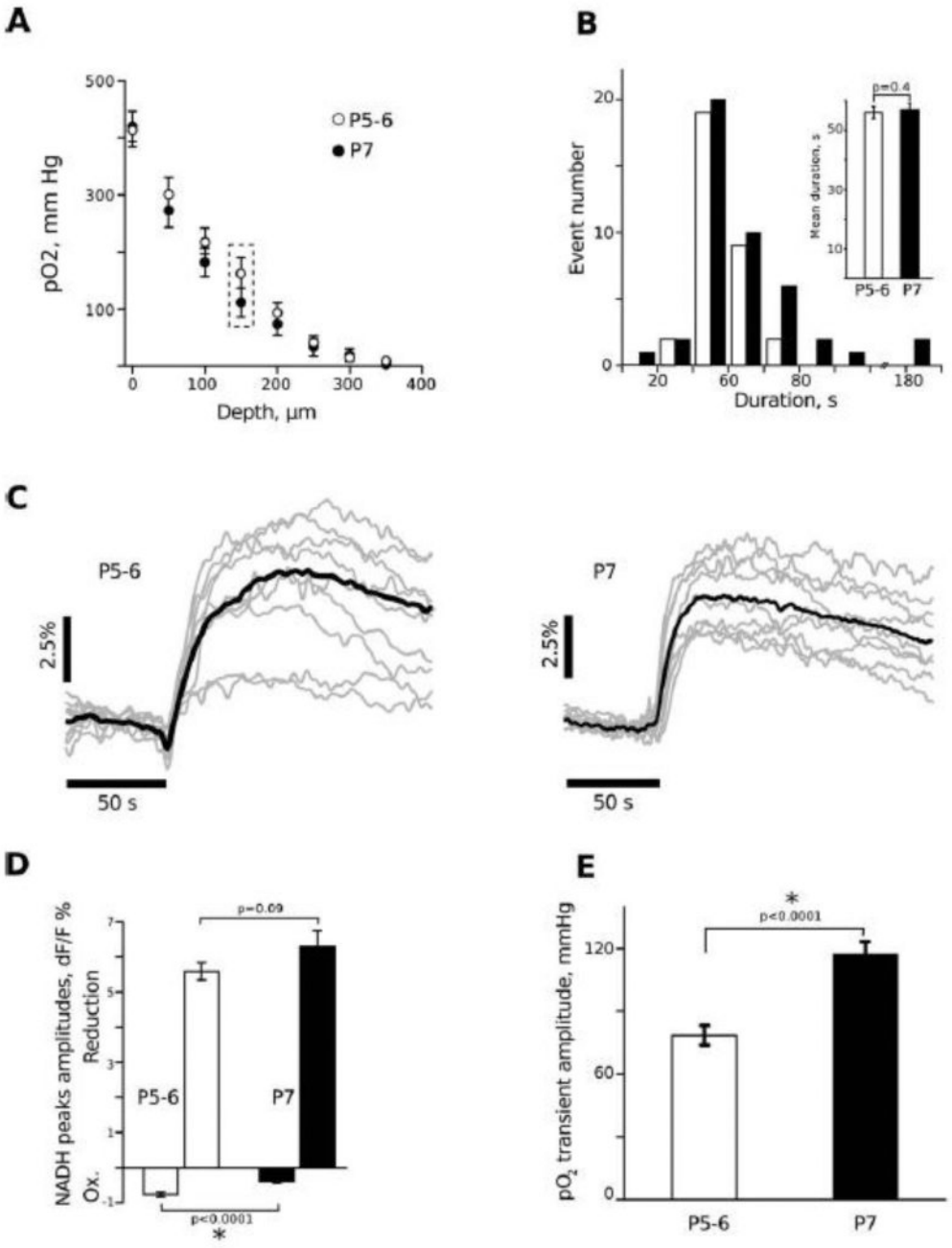

Figure 5. Tissue Oxygen Profiles and ILE Responses at P5 and P7

Panel A shows the depth profile associated with the submerged intact, immature hippocampi, beginning at the ventricular CA1 surface, which is positioned upwards within the chamber. At this age range (P5-P7) the entire depth of the CA1 region is within 150 µm from the surface, indicating that the region being recorded is well oxygenated, above the 100 mm Hg level at rest. The only difference between the two ages is at 150 µm depth. Panel B shows the duration of ILE events, which are similar at P5 and P7. Panel C shows details of individual ILE occurrences at P5 and P7, showing a trend to slightly more oxidation preceding the reduction at P5, confirmed with a bar plot in Panel D. Panel E shows that there

is enhanced oxygen transient with each ILE at P7, suggesting increased physiological synchronization and enhanced energy demand at P7 compared to P5, coincident with maturation of the tissue.

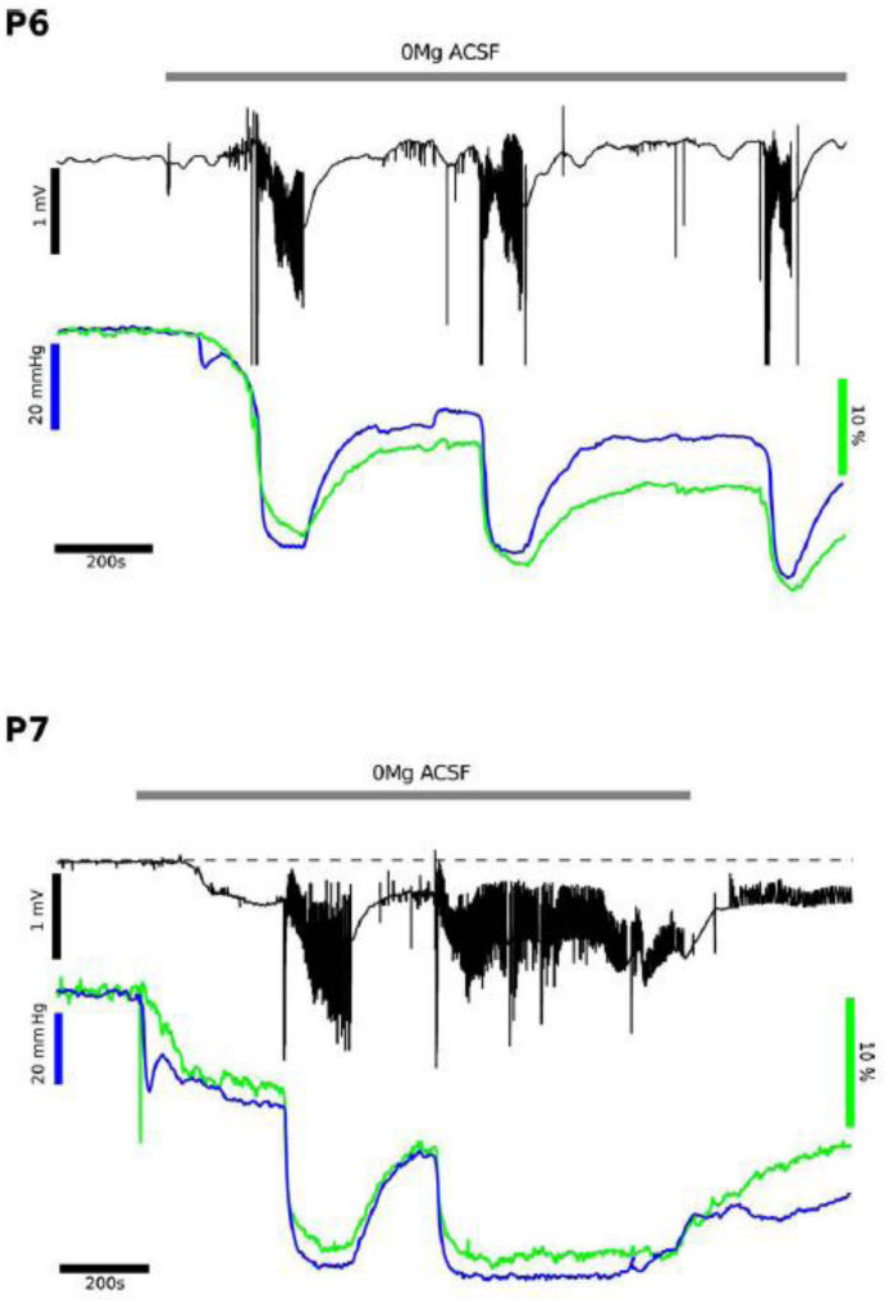

Figure 6. FAD and Tissue Oxygen Levels at P6 and P7

To complement the fluorescent NADH imaging (ie, Fig.'s 1,2,3) FAD imaging measurements (blue) were used in conjunction with field potential measurements (black) and tissue oxygen levels (green). In the upper panel the low Mg2+ conditions were tested at P6, showing repeated interictal like events (ILEs) with FAD showing primarily reduction events (ie, less oxidized FAD) and no initial oxidation with each ILE. At P7 the ILE event appears similar to P6, but once the late recurrent depolarization events begin then there is a persistent reduction (similar to the NADH), suggesting a high rate of ongoing metabolism,

as noted by the persistent low O2 level. These FAD recordings confirm the NADH fluorescence findings.

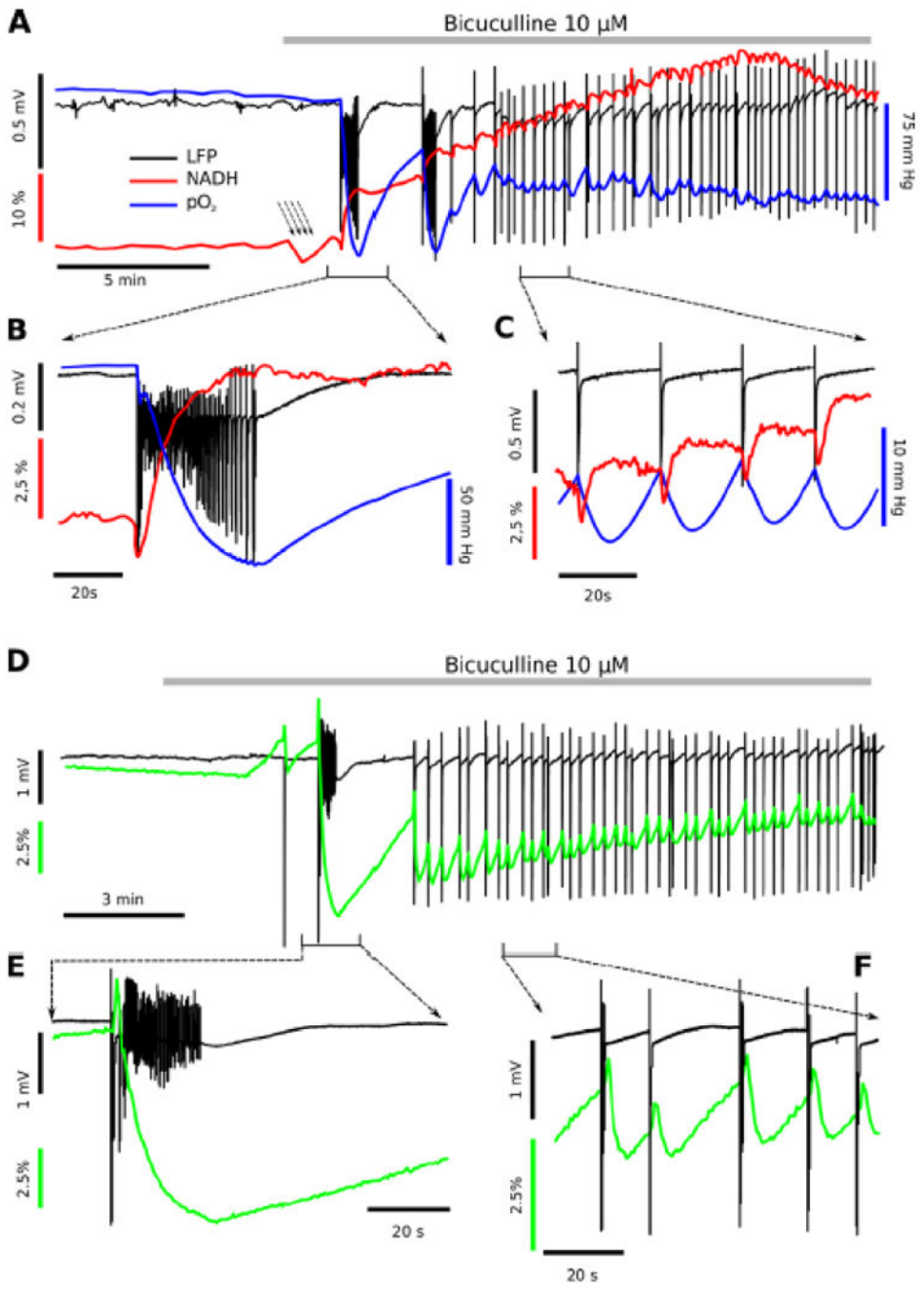

Figure 7. Bicuculline Epileptiform Responses

Application of the $GABA_A$ receptor inhibitor bicuculline (10 µM) induced interictal like events (IEs) and a slow, metabolic transition noted in the NADH, FAD+ and oxygen recordings. Panel A shows a comparison of electrical activity, NADH and tissue O2 levels. Bicuculline application induced first a decrease (-1.6 ± 0.4 %; $p<0.01$, N=6, A arrows) then a rapid rise in NADH fluorescence (average rate 0.8 ± 0.2 % per 10 s, A: red trace) and generation of either occasional, short ictal-like events (ILEs) or mainly interictal population spikes (A: black trace). Panel B demonstrates one detailed example of NADH imaging (red

trace) and pO2 profile (blue trace) corresponding to the first bicuculline - induced ILE (black traces), demonstrating an initial oxidation then a progressive reduction and profound O2 consumption as the abnormal epileptiform activity ensues. In contrast, Panel C shows the pattern of interictal responses most commonly noted in bicuculline, with small tissue oxygen and NADH fluorescence dips with each interictal response. Panel D shows an example of FAD+ recording corresponding to one ILE followed by multiple IEs. Panel E demonstrates one detailed example of FAD imaging (green trace) corresponding to the first bicuculline - induced ILE (black traces), demonstrating an initial oxidation (FAD peak) then a progressive reduction (FAD undershoot) during entire ILE. Panel F shows the pattern of FAD fluorescence induced by interictal events. Each IE is accompanied by biphasic FAD signal: fast peak (FADH2 oxidation) and slow undershoot (FAD reduction).

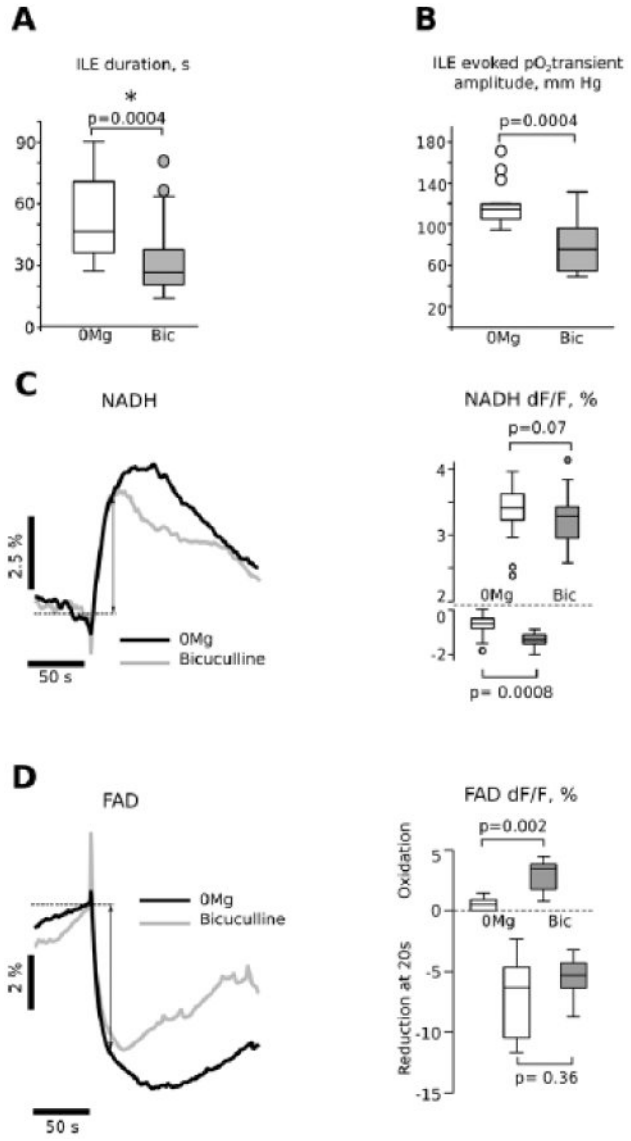

Figure 8. Comparison of Ictal-Like Events evoked in low Mg2+ aCSF or by bicuculline application

Panel A shows a comparison of ictal-like events (ILEs) from both low Mg2+ and bicuculline conditions, indicating that ILE duration was significantly longer in the low Mg2+ condition. Panel B shows a larger tissue oxygen transient in low Mg2+ conditions than with bicuculline-induced ILEs, likely due to the longer duration of the ILE events in low Mg2+ conditions (A). Panel C compares averaged NADH fluorescence responses for the two conditions. Although the NADH overshoot peak amplitude seems to be larger in low Mg2+ condition, it is mainly explained by a difference in ILE duration, because there is no difference in NADH relative fluorescence intensity at 20 s (mean duration of bicuculline induced ILE) after onset of the reduction phase (3.4+/-0.22% in low Mg2+ vs 3.3+/-0.42 in bicuculline; double head arrow on the averaged NADH traces shows where measurements were done). However, the mean oxidative dip was larger in bicuculline (-1.54 ± 0.1 % vs -1.03 ± 0.1 %; $p < 0.001$, $n = 14$). Panel D compares averaged FAD fluorescence responses

for the two conditions. As in the case of NADH overshoot the FAD undershoot time-course is similar in low Mg2+and bicuculline, at least during first 20 s (double head arrow on the averaged FAD traces and box plot on right hand side panel). The mean oxidative peak was significantly larger in bicuculline (2.85 ± 0.41 % n=11 vs 0.57 ± 0.20 %, n=8, left hand side panel).